Title

Genome editing of a rice CDP-DAG synthase confers multipathogen resistance

Journal

Nature, 618(7967)

ISSN

0028-0836

Authors

Sha, Gan

Sun, Peng

Kong, Xiaojing

et al.

Publication Date

2023-06-29

DOI

10.1038/s41586-023-06205-2

Peer reviewed

Published in final edited form as:

Nature. 2023 June ; 618(7967): 1017–1023. doi:10.1038/s41586-023-06205-2.

Genome editing of a rice CDP-DAG synthase confers multipathogen resistance

Gan Sha[1,2,3,4,17], **Peng Sun**[1,2,3,4,17], **Xiaojing Kong**[1,2,3,4], **Xinyu Han**[1,2,3,4], **Qiping Sun**[1,2,3,4], **Laetitia Fouillen**[5], **Juan Zhao**[1,2,3,4,15], **Yun Li**[1,2,3,4], **Lei Yang**[1,2,3,4], **Yin Wang**[1,2,3,4], **Qiuwen Gong**[1,2,3,4], **Yaru Zhou**[1,2,3,4], **Wenqing Zhou**[1,2,3,4], **Rashmi Jain**[6,7], **Jie Gao**[8], **Renliang Huang**[9], **Xiaoyang Chen**[1,2,3,4,16], **Lu Zheng**[1,2,3,4], **Wanying Zhang**[1,2,3,4], **Ziting Qin**[1,2,3,4], **Qi Zhou**[10], **Qingdong Zeng**[11], **Kabin Xie**[8], **Jiandi Xu**[12], **Tsan-Yu Chiu**[10], **Liang Guo**[8], **Jenny C. Mortimer**[7,13], **Yohann Boutté**[5], **Qiang Li**[8], **Zhensheng Kang**[11], **Pamela C. Ronald**[6,7,14,✉], **Guotian Li**[1,2,3,4,6,7,✉]

[1]National Key Laboratory of Agricultural Microbiology, Huazhong Agricultural University, Wuhan, China.

[2]Hubei Hongshan Laboratory, Huazhong Agricultural University, Wuhan, China.

[3]Hubei Key Laboratory of Plant Pathology, Huazhong Agricultural University, Wuhan, China.

[4]The Center of Crop Nanobiotechnology, Huazhong Agricultural University, Wuhan, China.

[5]Laboratoire de Biogenèse Membranaire, Université de Bordeaux, CNRS, Villenave-d'Ornon, France.

[6]Department of Plant Pathology and the Genome Center, University of California, Davis, Davis, CA, USA.

[7]Feedstocks Division, The Joint BioEnergy Institute, Emeryville, CA, USA.

✉ **Correspondence and requests for materials** should be addressed to Pamela C. Ronald or Guotian Li. pcronald@ucdavis.edu; li4@mail.hzau.edu.cn.

Author contributions G.L., G.S., P.S. and P.C.R. designed the experiments. G.L. and R.J. screened and analysed the genomic data of the *rbl1* mutant. G.S., P.S., X.K., X.H., Y.L., Y.W., Q.G., X.C. and L.Z. performed plant infection assays. G.S., X.K., X.H. and Y.W. performed DAB, ROS, salicylic acid, subcellular localization, RT–qPCR and GUS histochemical analyses. L.Y. and Z.Q. performed bioinformatics analysis. G.S., J.G., L.F., L.G., J.C.M., Y.B. and Q.L. performed lipidomics assays. Y.Z. and Y.W. performed chemical supplementation analyses of *rbl1*. G.S., Q.S., Q.G., Q. Zhou and T.-Y.C. performed yeast mutant complementation analyses. J.Z. and K.X. generated the CRISPR constructs. X.K., X.H., Y.L., W. Zhou, W. Zhang, Q. Zeng and Z.K. screened the edited lines. G.S., Y.W., R.H. and J.X. performed field trials and agronomic trait analyses. G.L. and G.S. drafted the manuscript and G.L., G.S., P.S., L.F., L.Z., L.G., K.X., J.C.M., Q.L., Y.B., Z.K. and P.C.R. revised the manuscript. All authors read and approved the final manuscript.

Competing interests G.L., G.S. and X.H. are coinventors on a provisional patent application no. 202111041400.3 filed by Huazhong Agricultural University entitled 'The OsRBL1 truncated protein and its application in balancing disease resistance and yield in rice' that covers *rbl1* and *rbl1*$^{\Delta 12}$ lines. The remaining authors declare no competing interests.

Supplementary information The online version contains supplementary material available at https://doi.org/10.1038/s41586-023-06205-2.

Peer review information *Nature* thanks Zuhua He and the other, anonymous, reviewer(s) for their contribution to the peer review of this work.

Online content

Any methods, additional references, Nature Portfolio reporting summaries, source data, extended data, supplementary information, acknowledgements, peer review information; details of author contributions and competing interests; and statements of data and code availability are available at https://doi.org/10.1038/s41586-023-06205-2.

Reporting summary

Further information on research design is available in the Nature Portfolio Reporting Summary linked to this article.

[8]National Key Laboratory of Crop Genetic Improvement, Huazhong Agricultural University, Wuhan, China.

[9]National Engineering Research Center of Rice (Nanchang), Key Laboratory of Rice Physiology and Genetics of Jiangxi Province, Rice Research Institute, Jiangxi Academy of Agricultural Sciences, Nanchang, China.

[10]BGI-Shenzhen, Shenzhen, China.

[11]State Key Laboratory of Crop Stress Biology for Arid Areas, Northwest A&F University, Yangling, China.

[12]Institute of Wetland Agriculture and Ecology, Shandong Academy of Agricultural Sciences, Jinan, China.

[13]School of Agriculture, Food and Wine, University of Adelaide, Glen Osmond, South Australia, Australia.

[14]Innovative Genomics Institute, University of California, Berkeley, Berkeley, CA, USA.

[15]Present address: College of Chemistry and Life Sciences, Sichuan Provincial Key Laboratory for Development and Utilization of Characteristic Horticultural Biological Resources, Chengdu Normal University, Chengdu, China.

[16]Present address: College of Plant Protection, Anhui Agricultural University, Hefei, China.

[17]These authors contributed equally: Gan Sha, Peng Sun.

Abstract

The discovery and application of genome editing introduced a new era of plant breeding by giving researchers efficient tools for the precise engineering of crop genomes[1]. Here we demonstrate the power of genome editing for engineering broad-spectrum disease resistance in rice (*Oryza sativa*). We first isolated a lesion mimic mutant (LMM) from a mutagenized rice population. We then demonstrated that a 29-base-pair deletion in a gene we named *RESISTANCE TO BLAST1* (*RBL1*) caused broad-spectrum disease resistance and showed that this mutation caused an approximately 20-fold reduction in yield. *RBL1* encodes a cytidine diphosphate diacylglycerol synthase that is required for phospholipid biosynthesis[2]. Mutation of *RBL1* results in reduced levels of phosphatidylinositol and its derivative phosphatidylinositol 4,5-bisphosphate (PtdIns(4,5)P_2). In rice, PtdIns(4,5)P_2 is enriched in cellular structures that are specifically associated with effector secretion and fungal infection, suggesting that it has a role as a disease-susceptibility factor[3]. By using targeted genome editing, we obtained an allele of *RBL1*, named *RBL1*$^{\Delta 12}$, which confers broad-spectrum disease resistance but does not decrease yield in a model rice variety, as assessed in small-scale field trials. Our study has demonstrated the benefits of editing an LMM gene, a strategy relevant to diverse LMM genes and crops.

Genome editing has been widely used in functional studies of genes but its potential for crop improvement has not yet been broadly utilized[4]. Rice, a staple food for half of the world's population, is amenable to genome-editing technologies, and the results can be tested in large-scale, low-cost field trials. Plant diseases cause severe losses in agriculture, threatening global food security[5]. Rice blast, for example, caused by the fungal pathogen

Magnaporthe oryzae, results in annual yield losses equivalent to feeding more than 60 million people worldwide[6]. Given this cost, cultivating crops with resistance to diseases, particularly broad-spectrum disease resistance, is highly desirable[7]. Despite the importance of this goal, only a small number of broad-spectrum disease-resistance genes have been cloned and used in the field, such as *Xa21* (ref. 8), *bsr-d1* (ref. 9), *pigm*[10], *IPA1* (ref. 11), *ROD1* (ref. 12) and *UMP1* (ref. 13) in rice, *Lr34* (ref. 14) and *PsIPK1* (ref. 15) in wheat, and *mlo*[16,17] in barley.

LMMs form hypersensitive response-like lesions (a form of programmed cell death) in the absence of pathogens[18]. They also often confer durable and broad-spectrum disease resistance, representing a potential source for breeding resistance. However, LMMs often lead to reduced yield, which is why the use of genes that confer LMM phenotypes (hereafter referred to as LMM genes) has not been fully exploited in plant breeding, because there is a lack of useful alleles.

Phospholipids are essential components of biological membranes and are involved in various biological processes, including development and response to both biotic and abiotic stress[19]. In phospholipid biosynthesis (Extended Data Fig. 1), phosphatidic acid and cytidine triphosphate are converted to cytidine diphosphate diacylglycerol (CDP-DAG) by CDP-DAG synthases (CDSs). CDP-DAG and *myo*-inositol are used to produce phosphatidylinositol through phosphatidylinositol synthases[20]. A varied number of phosphate groups can be added to phosphatidylinositol to synthesize different phosphatidylinositol phosphates, including PtdIns3P, PtdIns4P and $PtdInsP_2$. In particular, plant $PtdIns(4,5)P_2$ has been demonstrated to be a disease-susceptibility factor[3,21]. However, the role of phospholipids in rice immunity is largely unknown.

Mutant *rbl1* shows enhanced immunity

To identify previously undescribed LMM genes, we visually screened more than 1,500 whole-genome-sequenced fast-neutron mutagenized lines in the rice variety Kitaake[22]. One of the six identified LMMs, named *rbl1*, was of particular interest because it showed enhanced resistance to both *M. oryzae* and the bacterial pathogen *Xanthomonas oryzae* pv. *oryzae* (*Xoo*) (Fig. 1a–f), although it led to low fertility (Extended Data Fig. 2a). The infection rate (3.4%) of *M. oryzae* appressoria (the cells the fungus uses to infect plants) in *rbl1* is significantly reduced compared with infected Kitaake plants (79.8%) (Fig. 1g). The spread of fungal hyphae was restricted in *rbl1* compared with Kitaake at 72 h post-inoculation (hpi), possibly because the fungus triggers the accumulation of reactive oxygen species (ROS) in *rbl1* (Fig. 1h,i). Similarly, *rbl1* showed significant upregulation of ROS, accumulation of salicylic acid, and activation of plant defence-related genes (Extended Data Fig. 2b–d). These responses have previously been observed in other LMMs, including *EBR1* (ref. 23), *spl-D*[24] and *oscul3a*[25].

Genetic analysis of a segregating M_3 population of *rbl1* plants revealed that the lesion-mimic phenotype is controlled by a recessive locus (Extended Data Fig. 2e). Subsequently, we whole-genome-sequenced pooled DNA from three lesioned M_3 segregants using Illumina[22] and identified a 29-base-pair (bp) deletion in *RBL1* (LOC_Os01g55360) (Fig. 1j). The

deletion cosegregated with the LMM phenotype. The deletion overlaps the ninth exon–intron junction in the *RBL1* gene and causes an in-frame deletion of the ninth exon, resulting in a 19-amino-acid truncation at the conserved C terminus of RBL1 (ref. 26) (Fig. 1k,l). The truncation overlaps the CDS signature motif for ion binding[27], likely resulting in a loss of function for RBL1. Genetic complementation assays confirmed that *RBL1* is the causative gene (Fig. 1m–p and Extended Data Fig. 2f–g). Furthermore, *RBL1* is transcribed in all the tissues we examined, with the highest level in the leaf, and its expression was induced by *M. oryzae* infection (Extended Data Fig. 3).

RBL1 synthesizes CDP-DAG, a phosphatidylinositol precursor

Because *RBL1* homologues are highly conserved (Extended Data Fig. 4a–c), we used heterologous expression to study their biochemical function using the yeast *cds1* mutant (Fig. 2a). The *RBL1* gene driven by a galactose-inducible promoter was transformed into the *cds1* mutant. The resulting complemented yeast strain, cdsC, grew well on galactose-containing medium but not on glucose-containing medium, and RBL1 forms a homodimer in yeast (Fig. 2b). By using lipidomics analysis, we detected higher levels of phosphatidic acid and reduced levels of phosphatidylinositol and phosphatidylglycerol in yeast cells cultured in glucose-containing medium compared with those in galactose-containing medium (Fig. 2c). These results suggest that RBL1 functions as a CDP-DAG synthase, an integral membrane protein.

We next used lipidomics technology to investigate the function of RBL1 in rice. Levels of phosphatidic acid and DAG in *rbl1* rice are higher than those in Kitaake. By contrast, levels of phosphatidylinositol and phosphatidylglycerol were reduced by 71% and 49%, respectively (Fig. 2d). The reduction in phosphatidylinositol is the most striking result of the phospholipid alterations (Fig. 2e). To test whether exogenous supplementation of phospholipids could rescue the LMM phenotype, we performed chemical complementation assays and observed that exogenous supplementation of the medium with phosphatidylinositol, but not phosphatidylglycerol or PtdIns(4,5)P_2, postponed lesion formation in *rbl1*, whereas phosphatidic acid accelerated lesion formation (Extended Data Fig. 5a–d). Because respiratory burst oxidase homologue (RBOH) proteins are important for ROS generation[28], we applied the RBOH inhibitor diphenyleneiodonium chloride to *rbl1*. We observed that diphenyleneiodonium chloride could alleviate the LMM phenotype (Extended Data Fig. 5e).

To test whether increased production of phosphatidylinositol could rescue the LMM phenotype, we overexpressed rice *PIS1* (*OsPIS1*) in *rbl1*. These *OsPIS1* overexpression lines (*OsPIS1*::*rbl1*) accumulated 60- to 400-fold higher levels of *OsPIS1* transcript than did *rbl1* (Supplementary Table 1). Compared with *rbl1*, lesion formation in the *OsPIS1*::*rbl1* lines was reduced (Fig. 2f–i). Consistent with these results, Pathogenesis-related (*PR*) gene expression and resistance to *M. oryzae* in the *OsPIS1*::*rbl1* plants were lower than the levels observed in *rbl1* rice but higher than the levels in Kitaake (Fig. 2i,j). The phosphatidylinositol content of the *OsPIS1*::*rbl1* plants (0.817 nmol per mg dry weight) was restored to around 80% of that in Kitaake (1.017 nmol mg^{-1} dry weight), a significant increase from the *rbl1* line (0.319 nmol mg^{-1} dry weight; $P < 0.01$). We further analysed

the PtdInsP and PtdInsP_2 content and observed that their levels were fully restored in *OsPIS1*::*rbl1* lines from the reduced levels in *rbl1*, although the disease susceptibility was only partly restored (Fig. 2k). Similarly, we overexpressed the phosphatidic acid phosphohydrolase-encoding gene *OsPAH2* in *rbl1* (Fig. 2l). However, the *OsPAH2*::*rbl1* line, despite having restored phosphatidic acid content, showed only a minor reduction in the expression levels of *PR* genes and no alteration in lesion formation or resistance to *M. oryzae* (Fig. 2m–o), indicating that elevated levels of phosphatidic acid in *rbl1* contribute to enhanced immunity in only a limited way. We therefore focused on phosphatidylinositol derivatives in subsequent studies.

PtdInsP_2 in infection-specific structures

Using lipid blotting with PtdInsP_2-specific antibodies, we found a reduction in membrane PtdIns(4,5)P_2 in *rbl1* plants(Fig. 3a,b). To further analyse the spatiotemporal changes of PtdIns(4,5)P_2 in situ during fungal infection, we generated stable transgenic rice lines expressing the PtdIns(4,5)P_2 biosensor. PtdIns(4,5)P_2 was distributed evenly along the plasma membrane in Kitaake. In contrast, PtdIns(4,5)P_2 showed weak signals in the plasma membrane and was present in unknown intracellular vesicles in *rbl1* (Fig. 3c). Consistent with the western blotting results, membrane PtdIns(4,5)P_2 was reduced in *rbl1* compared with Kitaake on the basis of fluorescence signals (Fig. 3d,e). After infection by *M. oryzae*, PtdIns(4,5)P_2 quickly aggregated at the invasive hyphal tip like a cap (Fig. 3f). As the fungal infection progressed, PtdIns(4,5)P_2 was recruited to the extra-invasive hyphal membrane (EIHM) that encapsulates fungal infectious hyphae (Fig. 3g,h). Specifically, PtdIns(4,5)P_2 was enriched in an infection-specific structure called the biotrophic interfacial complex (BIC), as indicated by the fluorescent cytoplasmic effector Pwl2 (Fig. 3i), which is important for effector secretion and fungal infection[29]. PtdIns(4,5)P_2 was hardly observed in the cytoplasm of *rbl1*. The BIC formation rate was only 16.7% in *rbl1,* compared with 93.3% in Kitaake (Fig. 3j). Taken together, these results indicate that PtdIns(4,5)P_2 could have a role in interactions between the fungus and the rice (Fig. 3k).

RBL1$^{\Delta 12}$ balances growth and immunity

The *rbl1* line displays broad-spectrum disease resistance but has a roughly 20-fold reduction in yield (Extended Data Fig. 2a). To further evaluate the effects of different *RBL1* alleles on plant yield and immunity, we designed guide RNAs by using a multiplexing genome-editing strategy to target multiple sites in *RBL1* (Fig. 4a and Extended Data Fig. 6a–d). We obtained a total of 57 T_0-generation edited lines; 38 of them showed obvious LMM phenotypes and reduced seed sets, similar to *rbl1*; the other 19 displayed no or fewer lesions and varied seed sets in the greenhouse (Fig. 4b). Notably, the *rbl1*$^{\Delta 12}$ line with a 12-bp deletion, which showed only tiny hypersensitive response-like lesions starting at the booting stage (Fig. 4c, Extended Data Figs. 7a and 8), produced a normal seed set (Fig. 4d). Detailed infection assays revealed that *RBL1*$^{\Delta 12}$ conferred resistance to 10 *M. oryzae* field strains, 5 *Xoo* strains and 2 rice false smut *Ustilaginoidea virens* strains (Fig. 4e–j). Accordingly, the levels of mycotoxins in spikelets infected by *U. virens* were reduced by 66.2% in *rbl1*$^{\Delta 12}$ compared with those in Kitaake (Fig. 4i).

We next performed small-scale field trials aimed at assessing the usefulness of *RBL1*$^{\Delta 12}$ with transgene-free seeds (Extended Data Fig. 6e–g). The grain yield of *rbl1*$^{\Delta 12}$ was evaluated in four fields in three provinces (18° 41′–30° 47′ N) in primary rice-production areas of China where no or little *M. oryzae* was present. Multiple key agronomic traits were assessed, including plant height, tiller number per plant, seed setting rate, thousand-grain weight and grain yield. We found that, except for plant height, all measured traits were similar for *rbl1*$^{\Delta 12}$ and Kitaake (Extended Data Fig. 6h); *rbl1*$^{\Delta 12}$ yielded 1.66 kg of grains per hundred plants, compared with 1.70 kg of grains for Kitaake (Fig. 4k). In a fifth location (Enshi) with a high incidence of *M. oryzae*, the *rbl1*$^{\Delta 12}$ plants displayed robust resistance to both leaf and panicle blast. The severity of panicle blast for *rbl1*$^{\Delta 12}$ plants was 15.8%, much lower than that of Kitaake, which was 90.3%. Regarding yield, we found that *rbl1*$^{\Delta 12}$ yielded 5.3-fold more grains than the control Kitaake plants that were severely damaged by blast (0.75 kg compared with 0.12 kg per hundred plants) (Fig. 4l,m). Taken together, these results demonstrate that the *RBL1*$^{\Delta 12}$ allele in Kitaake rice confers robust broad-spectrum disease resistance with no reduction in yield in a small-scale field trial.

We next analysed the *RBL1*$^{\Delta 12}$ allele in detail. The four amino acids truncated in RBL1$^{\Delta 12}$ are conserved in plants (Extended Data Fig. 7b). The increased level of ROS in *rbl1*$^{\Delta 12}$ when challenged with chitin is within the range of other rice cultivars (Extended Data Fig. 7c). The 12-bp deletion caused a significant reduction in gene expression, although no alteration in protein thermostability or subcellular localization was observed (Extended Data Fig. 7d–i). *RBL1* complements the *rbl1*$^{\Delta 12}$ line but the *RBL1*$^{\Delta 12}$ allele does not complement *rbl1* (Extended Data Fig. 7j–l). The complementation result was confirmed in the F_2 population derived from Kitaake crossed with *rbl1*$^{\Delta 12}$, which also indicates that the *RBL1* locus contributes to resistance in a reverse dosage-dependent manner (Extended Data Fig. 7m–o). The PtdInsP_2 levels and BIC formation rate were reduced in the *rbl1*$^{\Delta 12}$ line compared with Kitaake (Extended Data Fig. 7p–s). These results indicate that the *RBL1*$^{\Delta 12}$ allele results in a four-amino-acid truncation and a reduction in *RBL1*$^{\Delta 12}$ gene expression. We also generated *RBL1* edited lines in two other rice cultivars, Nipponbare and Zhonghua 11, and observed increased resistance to *M. oryzae* and normal growth, similar to *rbl1*$^{\Delta 12}$ (Extended Data Fig. 9).

Discussion

These results reveal a connection in rice between phospholipid metabolism and disease resistance. They further indicate important functions of RBL1, a CDP-DAG synthase, in the control of programmed cell death and immunity through the regulation of phosphatidylinositol biosynthesis. In *Arabidopsis thaliana*, the knockdown *cds* mutants showed enhanced immunity (Extended Data Fig. 4d–i)[30]. These data suggest that *RBL1* homologues have conserved roles in immunity. The mutation of *OsCDS5* has been shown to enhance the tolerance of rice to hyperosmotic stress[31]. Taken together, the findings suggest that CDSs have broad roles in plant biotic and abiotic stress responses. Phosphatidylinositol derivatives often have crucial roles in biology[32]. The amount of PtdIns(4,5)P_2 is reduced in both *rbl1* and *rbl1*$^{\Delta 12}$ plants. PtdInsP and PtdInsP_2 have been shown to be involved in immunity in both plants and animals[33–35]. Our results specifically show that PtdIns(4,5)P_2 is enriched in the BIC and EIHM (Fig. 3i), structures involved in effector secretion and *M.*

oryzae infection[29]. This observation is consistent with studies reporting that PtdIns(4,5)P_2 serves as a disease-susceptibility factor that is recruited to infection sites to facilitate infection[3,21]. The exact role of PtdIns(4,5)P_2 and PtdInsP in fungal effector secretion, rice immunity and the relevant regulatory mechanisms[36] needs further investigation, however.

The *RBL1*$^{\Delta 12}$ allele in a model rice variety confers broad-spectrum disease resistance but does not reduce yield in small-scale field trials. Our results indicate that the fine-tuning of host factors involved in the formation of infection-specific structures is a strategy for balancing immunity and yield. Our observations of the performance of the *rbl1*$^{\Delta 12}$ plants are promising. Multi-year field trials are now needed to evaluate the performance of the *RBL1*$^{\Delta 12}$ allele in elite, locally adapted rice varieties.

Like the disease-resistance genes *Lr34* and *mlo, RBL1* was isolated from LMMs. *Lr34* and *mlo* are highly conserved and have been applied to multiple crops for disease resistance[37,38]. Similarly, the *RBL1* homologues in other crops should be investigated further. LMM genes, which often encode negative regulators of immunity, represent an important class of genes conferring broad-spectrum disease resistance[7,39]. Negative regulators are particularly compatible with genome-editing technologies that can efficiently create complete or partial loss-of-function alleles[40,41]. With continued advances in genome-editing technologies[1], the strategy we have demonstrated in this study will become increasingly valuable to diverse LMM genes and crops.

Methods

Plant materials, strains and growth conditions

The *rbl1* mutant FN398 was identified from a fast-neutron (FN)-induced mutant population generated in the model *japonica* rice (*O. sativa*) line KitaakeX[42]. The genome sequence of KitaakeX is available online (https://phytozome.jgi.doe.gov/pz/portal.html)[43]. The segregating M_3 population derived from the *rbl1* line was used in sequencing and cosegregation assays. For infection assays and other phenotype characterizations, rice seeds were surface-sterilized and germinated on 1/2 Murashige and Skoog (MS) medium. After a week in the growth chamber, plants were transferred to the greenhouse with a photoperiod of 12:12 h light:dark at 28 °C. *Arabidopsis* plants were cultivated in potting soil mix (peat soil:rich soil:vermiculite of 1:1:1, v/v/v) in the growth chamber at 21 °C, 60% humidity, with a day:night period of 16:8 h and an intensity of 80 μmol m^{-2} s^{-1} (refs. 30,44). *X. oryzae* pv. *oryzae* (*Xoo*) strains were grown on nutrient broth plates at 28 °C for 3 days before use[45]. *M. oryzae* strains were cultured on oatmeal agar plates under light at room temperature[46,47]. *U. virens* strains were routinely grown on potato saccharose agar (PSA) plates and were grown in the potato saccharose broth (PSB) medium at 28 °C, 160 rpm for 7 days for conidiation[48]. The *P. capsici* strain was cultured on potato dextrose agar (PDA) plates at 25 °C for 3–4 days in the dark before use[49].

Tagging *M. oryzae* strains with fluorescence proteins

Fungal protoplast preparation and transformation were performed as previously described[50]. In brief, the GFP overexpression plasmid RP27–GFP, the apoplastic effector Bas4–mCherry

vector that was used to indicate the EIHM, and the cytoplasmic effector Pwl2–mCherry vector that was used to indicate the BIC were transformed into *M. oryzae* strain ZB25 (refs. 29,51). The resultant transformants were selected on TB3 (yeast extract 6 g l^{-1}, casamino acid 6 g l^{-1}, sucrose 200 g l^{-1}, agar 18 g l^{-1}) plates with 500 μg ml^{-1} geneticin (GLPBIO). The neomycin-resistant transformants were verified using PCR and examined by laser scanning confocal microscopy.

Plant infection assays

The leaf-clipping method was used for *Xoo* infection of rice plants at the booting stage[52]. *Xoo* cultures of strains PXO71, PXO99, PXO341, ZHE173 and GX01 (ref. 53) were suspended in distilled water and the bacterial suspension concentrations were adjusted to an optical density at 600 nm (OD_{600}) of around 0.5. Sterilized scissors were dipped into the bacterial suspension and were used to cut the leaves 5 cm from the leaf tip. Infected plants were transferred to the greenhouse. The greenhouse was set to a day:night period of 12:12 h, a temperature of around 28 °C and a relative humidity of 80%. Water-soaked lesions were scored at 14 dpi or as indicated in the figure legends. At least three plants were inoculated for each experiment. The *ΔraxST Xoo* strain that can overcome the XA21-mediated immunity was used to infect the KitaakeX line carrying the *Xa21* gene[53].

M. oryzae strains ZB25, LN3, LN13, LN14, ES18, ES24, ES28, ES36, ES76 and ES80 were isolated from rice fields in Enshi (ES) and Liaoning (LN) in China and stored in the laboratory. Punch inoculation was done as previously described[54]. In brief, spores were freshly collected from 10-day-old oatmeal agar cultures and the concentration was adjusted to 1×10^5 spores per ml with 0.025% Tween-20. Fully extended rice leaves at 30 days post-sowing (dps) were wounded with a punch and inoculated with 10 μl spore suspension. The punched area was sealed with clear Scotch tape. Inoculated plants were transferred to the greenhouse. Symptoms were scored at 14 dpi and relative fungal biomass abundance was measured using qPCR[25]. Primers used in the assay are listed in Supplementary Table 2.

For microscopy analysis of *M. oryzae* infection, the ZB25–eGFP strain stably expressing GFP was used to inoculate detached rice sheaths of 5-week-old rice plants. The spore concentration was adjusted to approximately 1.5×10^6 conidia per ml. The fungal infection rate in each plant was analysed from five replicates at 72 hpi, and at least 30 appressoria for each replicate were examined for invasive hyphae growth in the rice sheath cells by laser scanning confocal microscopy (Leica TCS SP8).

For false smut infection with *U. virens* strains HWD2 and JS60 (ref. 55), panicles of rice plants at the booting stage were inoculated with 1 ml of a mixture of spores and homogenized mycelia with a syringe. Infected plants were kept at around 25 °C with about 85% relative humidity in the greenhouse. The number of smut balls per panicle was counted at 17 dpi. Spikelets were sampled from the Kitaake and *rbl1*$^{\Delta 12}$ lines inoculated at 36 h, 72 h and 7 d, and were examined with a scanning electron microscope (JSM-6390/LV) as previously described[56].

Infection assays in *Arabidopsis* with *P. capsici* were conducted as previously described with minor modifications[49]. In brief, *P. capsici* strain LT263 was cultured on PDA plates

for 3 days at 25 °C in the dark. Detached leaves of *Arabidopsis* at 30 dps were placed on 0.8% water–agar plates and inoculated with 3 mm × 3 mm blocks of the *P. capsici* culture. The samples were kept at room temperature in the dark. The inoculated leaves were photographed under ultraviolet light and the lesion area and relative pathogen biomass were measured at 36 hpi.

DAB staining

To visualize hydrogen peroxide in plant tissue, rice leaves were collected at 40 dps and immediately immersed in 3,3′-diaminobenzidine (DAB) staining solution (1 mg ml^{-1}) in 15-ml tubes. The tube was covered with aluminium foil and incubated with shaking at 80–100 rpm at room temperature for 8 h. Samples were decoloured with 95% ethanol in a boiling-water bath for 10 min and bleached for another 48 h in fresh 95% ethanol until most of the chlorophyll had been removed from the sample. The cleared leaves were then visualized for DAB staining.

Measurement of ROS

ROS was measured after chitin treatment as previously described[25]. In brief, rice plants were grown on 1/2 MS medium in the growth chamber for 12 days. Leaves of the seedlings were cut into disks (3 mm × 3 mm) and then submerged in distilled water in a 96-well plate under light overnight. The distilled water was pipetted out and replaced with 100 μl of mixed solution for each well (the solution contained 50 μM luminol (Wako), 10 μg ml^{-1} horseradish peroxidase and 8 nM chitin (GLPBIO)) using a multiple-channel pipette. Chemiluminescence was measured at 500-ms intervals over a period of 40 min in a SPARK-10M microplate reader (TECAN). Eight biological replicates were used for each sample. Distilled water was used as the mock control.

Quantification of total salicylic acid in leaves

For the measurement of total salicylic acid, plants were grown on 1/2 MS medium in the growth chamber for 12 days, after which leaf tissues were harvested and freeze-dried. About 20 mg of dried tissue was ground in liquid nitrogen. The sample powder was mixed with 1 ml 80% (v/v) methanol using an ultrasonic cleaner at 70 °C for 15 min. The mixture was centrifuged at 7,000*g* at 4 °C, and the supernatant was collected and filtered (with a filter diameter of 0.22 μm). Salicylic acid in the samples and serial dilutions of the salicylic acid standard were analysed together using high-performance liquid chromatography and tandem mass spectrometry. The salicylic acid content of each sample was calculated by comparing with the calibration curve of the salicylic acid standard.

RNA extraction and RT–qPCR

Rice leaves were frozen in liquid nitrogen. RNA was isolated with TRIzol (CWBIO). Residual DNA was eliminated with DNase I (Thermo Scientific). Purified RNA was examined using agarose gel electrophoresis before complementary DNA (cDNA) synthesis, which was performed using the HiScript II 1st Strand cDNA Synthesis Kit (Vazyme). RT–qPCR was performed on a Bio-Rad CFX96 Real-Time System coupled to a C1000 Thermal Cycler (Bio-Rad) using SYBR Green mix (Vazyme). Gene-expression analysis was

performed using CFX Manager (Bio-Rad). The $2^{-\Delta\Delta Ct}$ method was used to calculate the expression level of target genes[57]. Three biological replicates were used for each sample. The rice *ACTIN* gene (LOC_Os03g50885, NM_001058705) was used as the internal control with various primers (Supplementary Table 2).

Cloning of *RBL1* and genetic complementation

The *rbl1* mutant was crossed with Kitaake and the resulting F_1 plants were examined for the spontaneous lesion phenotype to assess if the phenotype was controlled in a recessive or dominant manner. DNA was isolated from pooled samples of three M_3 plants showing spontaneous lesions. Genomic sequencing, performed on a HiSeq 2500 next-generation sequencing system (Illumina), and mutation identification, using the established bioinformatic pipeline, were conducted as described[22]. Insertion and deletion (InDel) markers for identified homozygous mutations were used in a cosegregation assay (Supplementary Table 2). Primers RBL1cDNAF/R were used to amplify the coding sequence of *RBL1* from cDNA of Kitaake and the *rbl1* mutant, and the resultant products were sequenced. To complement the *rbl1* mutant, the entire open reading frame of the *RBL1* gene, including its native 2-kb promoter sequence upstream of the start codon ATG, was amplified using PCR with primers CORBL1F/R (Supplementary Table 2). The PCR product was purified and then cloned into the binary vector pCAMBIA2300 using a HiFi DNA Assembly Master Mix (NEB). The resultant construct was confirmed using Sanger sequencing. Subsequent *Agrobacterium*-mediated transformation and transformant selection were performed at BioRun BioScience. Positive transformants were examined using the marker for cleaved amplified polymorphic sequences (Supplementary Table 2). *RBL1* expression and fungal infection assays were done as described above.

Yeast mutant complementation and protein purification

The *RBL1* open reading frame was amplified from Kitaake cDNA with primers YCF1/R1 (Supplementary Table 2) and cloned into plasmid pYES2-His as pYES2-RBL1-His. Competent cells of the yeast strain BY4741 (*MATa*, *his3*, *leu2*, *met15*, *ura3*) (WT) were prepared and transformed with the pYES2-RBL1-His construct using the Super Yeast Transformation Kit (Coolaber). The Ura^+ transformant was confirmed using PCR and then used to knock out the yeast endogenous *cds1* gene using a homologous recombination approach[58]. The resultant strains were confirmed using PCR and assayed for growth on YPD and YPGal plates at 30 °C. To analyse the RBL1 protein expression in yeast, the total protein was isolated from the complementation and wild-type strains, and the His-tagged RBL1 protein was detected using western blotting with anti-His-tag antibody (1:5,000; Cell Signaling Technology). Western blotting was performed following the manufacturer's instructions. Functional complementation assays with the RBL1–GFP fusion protein were performed similarly.

For protein expression and purification, total proteins were isolated from yeast strains BY4741 and transformants carrying pYES2–*RBL1*–6×His and pYES2–*RBL1*$^{\Delta 12}$–6×His. The 6×His-tagged RBL1 and RBL1$^{\Delta 12}$ proteins were purified from total proteins using the Ni-NTA protein purification system according to a method described previously[2]. The thermostability assays of the fusion proteins were performed using a differential scanning

calorimeter as previously described[59]. In brief, the temperature range was set from −100 °C to 150 °C, and the scan rate was 60 °C per h.

Yeast lipidomics assays

To analyse the functions of RBL1 in yeast, the wild-type and complementation yeast strains were cultured in YPGal to reach an OD_{600} of around 0.6, and the yeast cells were collected using brief centrifugation and rinsed with sterile water once. The yeast cells were then resuspended in YPD or YPGal and cultured at 30 °C, 220 rpm for up to 4 h, 8 h and 20 h before collection for phospholipid isolation. The yeast cells were then homogenized with acid-washed glass beads, and 1 ml extraction buffer chloroform:methanol:formic acid (10:10:1, v/v/v) was added to the homogenized yeast cells and vortexed for 3 min and centrifuged at 4 °C, 1,000*g* for 6 min to collect the supernatant. The extraction was repeated once with chloroform:methanol:water (5:5:1, v/v/v). The supernatant was combined and mixed well with 3 ml buffer (0.2 M H_3PO_4, 1 M KCl). The mixture was centrifuged at 4 °C, 1,000*g* for 10 min. The lower organic phase was collected and dried under the nitrogen gas. The dried sample was dissolved in 300 μl chloroform and lipid extracts were analysed using liquid chromatography and mass spectrometry as previously described[60].

Protein subcellular localization analysis

The full-length coding sequence of *RBL1* was amplified with primers SLRBL1F/R (Supplementary Table 2) and fused with the eGFP sequence in vector pEarleyGate101 under control of the CaMV 35S promoter[44]. The resultant constructs were confirmed using Sanger sequencing and transformed into *Nicotiana benthamiana* leaves with and without related marker constructs. For *N. benthamiana* transient expression, constructs were transformed into *Agrobacterium* strain GV3101 and the resultant strain was infiltrated into leaves of 30-day-old *N. benthamiana* plants. The fluorescence signal was observed with laser scanning confocal microscopy (Leica TCS SP8) 72 h after infiltration.

GUS histochemical assay

For the β-glucuronidase (GUS) activity assay, the 2-kb genomic region upstream of the start codon of *RBL1* was amplified by PCR from rice genomic DNA with the primers ProRBL1-F/R (Supplementary Table 2) and cloned into the pGreenII 0179-GUS vector[44]. The resultant construct, pRBL1–GUS, was confirmed using Sanger sequencing and transformed into rice calli using the *Agrobacterium*-mediated approach. Plants containing pRBL1–GUS were genotyped before GUS staining. For GUS staining, rice plant tissues were stained in the Ready-to-use GUS Staining Solution (PHYGENE) at 37 °C overnight. The stained plant tissues were rinsed with water and incubated in 70% ethanol for 24 h to remove the chlorophyll. Photomicrographs were taken using a stereoscopic microscope (Nikon SMZ1000).

Lipid extraction and analysis

Leaf samples from 5-week-old plants were used for the total phospholipid extraction as described previously[31]. In brief, more than 10 mg (fresh weight) rice leaf tissue was harvested and immediately immersed in preheated isopropanol (75 °C) with 0.01% butylated

hydroxytoluene and incubated for 15 min. After cooling to room temperature, chloroform was added to the sample and incubated with shaking at room temperature for 1 h. The lipid extracts were transferred to new glass tubes to repeat the extraction procedure until the leaf sample became bleached. The lipid extracts were combined and evaporated under nitrogen gas and then redissolved in chloroform. The lipidomics analysis was performed as described previously[61] using triple time-of-flight mass spectrometry with an electrospray ionization source in positive-ion mode. Lipids in each class were quantified by comparison with internal standards (Avanti).

Phosphoinositides were extracted as described previously[62]. In brief, lipids from dried leaf samples of the Kitaake, *rbl1*, *rbl1*$^{\Delta 12}$ and *OsPIS1*::*rbl1* lines were extracted with 750 μl methanol:chloroform:1 M hydrochloric acid (2:1:0.1, v/v/v) and 150 μl water in the presence of internal standards. Lipids were modified with trimethylsilyldiazomethane for 10 min. Liquid chromatography with tandem mass spectrometry (multiple-reaction-monitoring mode) analyses were performed using a QTRAP 6500 mass spectrometer (ABSciex) coupled with a liquid chromatography system (1290 UPLC Infinity II, Agilent). Analyses were done in positive-ion mode. Reverse-phase separations were carried out on a Jupiter C4 column (50 × 1 mm; particle size, 5 μm; Phenomenex). Eluent A was water and 0.1% formic acid, and eluent B was acetonitrile and 0.1% formic acid. The gradient elution program was as follows: 0–2 min, 45% eluent B; 2–27 min, 45–100% eluent B; and 27–30 min, 100% eluent B. The flow rate was 100 μl min^{-1}; 10-μl sample volumes were injected. The area of liquid-chromatography peaks was determined using MultiQuant and PeakView software (ABSciex) for relative quantification to the area of the internal standard, and values are expressed in arbitrary units by quantity (dry weight).

Chemical supplementation and overexpression of *OsPIS1* and *OsPAH2*

Phospholipids, phosphatidylglycerol, PtdIns(4,5)P_2 and diphenyleneiodonium chloride were added to DMSO and incubated at 42 °C for 30 min and were treated in the ultrasonic homogenizer for 10 min to facilitate the dissolving. The mixture was filter-sterilized (filter diameter, 0.22 μm). For chemical supplementation assays, Kitaake and *rbl1* plants were grown on 1/2 MS medium with phosphatidylinositol (0, 10, 50 and 100 μM), phosphatidylglycerol (0, 10 and 100 μM), PtdIns(4,5)P_2 (0, 50 and 100 nM), phosphatidic acid (0, 0.1, 1 and 10 μM), or diphenyleneiodonium chloride (0, 0.1, 0.5 and 1 μM) in the growth chamber for about 6–10 days. The leaves were then examined for lesions for a further 10 days. To overexpress *OsPIS1* and *OsPAH2*, genomic regions of these two genes were cloned into vector pRGV under control of the maize *UBIQUITIN10* promoter[63]. The resultant constructs were sequenced and transformed into the *rbl1* mutant. The overexpression lines were genotyped, analysed using RT–qPCR and examined for lesions. Plant infection assays and related RT–qPCR assays of the overexpression line were performed as described above.

Plasma-membrane extraction and lipid-blotting assays

The enrichment and purification of plasma membranes were performed using aqueous two-phase partitioning as described previously[64]. In brief, rice leaves (20 g) were homogenized in liquid nitrogen and were immediately added to 120 ml ice-cold buffer (50 mM Tris-Me

(pH 8.0), 0.25 M sucrose, 3 mM EDTA, 0.6% PVP, 10% glycerol, 10 mM DTT, 1 mM PMSF and 1 × protease-inhibitor cocktail). When the homogenized tissues were obtained, one small portion of the sample was used to extract proteins for the loading control; the primary antibody was anti-plant ACTIN mouse monoclonal antibody (1:2,000, Abbkine), the remaining sample was used to extract membrane lipids. The samples were centrifuged at 60,000*g* for 30 min to pellet plasma membrane vesicles. The plasma membrane was then mixed with 1 ml chloroform:methanol:c oncentrated HCl (1:2:0.02, v/v/v) solution, and the lipid components were separated using 300 μl chloroform and 300 μl KCl (2 M).

For subsequent lipid dot blotting, the organic phase was applied to a nitrocellulose filter membrane and $PtdInsP_2$ was detected using the mouse anti-$PtdInsP_2$ antibody 2C11 (1:2,000, Abcam), as described previously[65]. ImageJ software was used to quantify the content of $PtdInsP_2$ on the blotted membrane.

Subcellular localization and fluorescence intensity assays of rice PtdInsP and $PtdInsP_2$

A set of vectors that genetically encodes biosensors for PtdInsP and $PtdInsP_2$ from the Nottingham Arabidopsis Stock Centre were used, including mCIT-2 ×$FYVE^{HRS}$ for PtdIns3P, mCIT-2×PH–FAPP1 for PtdIns4P and mCIT-1×$PH^{PLC\Delta1}$ for PtdIns(4,5)P_2 (ref. 66). To analyse the subcellular localization of PtdInsP in rice protoplasts, we cloned the 1×$FYVE^{HRS}$, 1×PH–FAPP1 and 1×$PH^{PLC\Delta1}$ fragments into the pM999–eGFP vector under control of the CaMV 35S promoter. The resultant constructs were confirmed using Sanger sequencing and transformed into rice protoplasts. Preparation and transformation of the rice protoplasts were performed as described[67]. The fluorescence intensity of PtdInsP was quantified using ImageJ as described previously[62]. The ratio of the signals at the plasma membrane to total fluorescence signals was calculated.

To generate rice lines that stably express genetically encoded biosensors for PtdIns(4,5)P_2, we cloned the 1xPH–PLCΔ1 fragment into the pRGV–eGFP vector under control of the maize *UBIQUITIN10* promoter[63]. The resultant vector was verified by sequencing and transformed into Kitaake and *rbl1*$^{\Delta12}$, which were further crossed with *rbl1*. Confocal laser scanning microscopy was performed (Leica TCS SP8). Intactness of the PtdIns(4,5)P_2 biosensor in rice was examined using western blotting as described previously[68]. In brief, rice leaf tissues were ground to a fine powder with a pestle and mortar in liquid nitrogen and solubilized in the extraction buffer (50 mM Tris-HCl, pH 7.5, 150 mM NaCl, 1 mM EDTA, 1% Tritonx-100, 0.5 mM PMSF and 1% protease inhibitor cocktail). The protein extracts were centrifuged at 12,000*g* at 4 °C and the supernatant was cleared through a filter (diameter, 0.45 μm). We mixed 70-μl protein exacts, 10 μl 0.4 M DTT, 20 μl 5×SDS loading buffer and 1 μl β-mercaptoethanol, and took a 20-μl mixed sample to run 10% SDS–PAGE. The blotting was performed on a PVDF membrane (Bio-Rad). The primary antibody was anti-GFP (1:2,000, Cell Signaling Technology). Coomassie brilliant blue staining of rice ribulose bisphosphate carboxylase/oxygenase (RUBISCO) was used as the internal control[69].

To analyse the subcellular localization of rice PtdIns(4,5)P_2 during *M. oryzae* infection, the verified T_2 plants were used to analyse subcellular locations of PtdIns(4,5)P_2 in rice sheath cells[70], inoculated with the *M. oryzae* ZB25 strains expressing Pwl2–mCherry or

Bas4–mCherry. The fluorescence signal was detected using a confocal microscope (Nikon N-STORM) with the following settings of excitation and emission wavelengths: GFP (488/505 and 530 nm) and mCherry (561/587 and 610 nm).

Genome editing

Genome editing of *RBL1* was conducted using a previously described method[71]. In brief, guide RNAs for genome editing were selected, assisted by the online program CRISPR-Plant[72]. Related primers were designed (Supplementary Table 2) and the guide RNA cassette was assembled into vector pBER32 as described[71]. After confirmation by Sanger sequencing, the binary constructs were transformed into embryogenic calli of Kitaake, Nipponbare and Zhonghua11 using *Agrobacterium*-mediated transformation. The resultant transformants were genotyped using Sanger sequencing and the sequence was analysed using SnapGene and DSDecodeM[73]. The confirmed edited lines were analysed for plant growth, *RBL* expression and plant-immunity phenotypes.

Field trials of the edited lines

Field yield was assessed at the Hainan, Hubei and Jiangxi experimental stations (low incidence of rice blast) and resistance to blast was evaluated in the Enshi blast nursery (high incidence of rice blast) in the summer season. Enshi (at Hubei) was selected because this mountainous area has a high incidence of rice blast disease each year[10]. Field plots was designed following the strategy established by the International Rice Research Institute[74]. For each field trial, plants were grown with either 10 (at Hainan) or 5 (at Hubei and Jiangxi) replicate plots for each line, and each plot contained 100 plants that were 20 cm apart. Diseased plantlets of the blast-susceptible line Lijiangxintuanheigu were used as a source of inoculum for spreading the disease[75]. One row of Lijiangxintuanheigu was sown for every 10 rows of test accessions, and the disease was allowed to spread naturally by wind dispersal. In the normal fields, we did not include a spreader row. Rice blast resistance of different lines was evaluated according to the International Rice Research Institute evaluation system, and the percentage of necrotic panicles caused by blast was calculated[74].

Quantification and statistical analysis

Sample sizes were chosen on the basis of previous publications as described in each section. Unless specifically stated, the sample size n indicates the number of biological replicates. Statistical analyses of lesion length, lesion area, pathogen biomass, infection rate, ROS accumulation, gene expression, lipid content, fluorescence intensity, grain production and other measurements were done using Graphpad Prism 8 and IBM SPSS Statistics 22 software. All values are presented with mean ± s.e.m. except Fig. 2j. Statistical significance was assessed using the two-tailed Student's *t*-test or Duncan's new multiple range test. No methods were used for sample randomization or to estimate sample sizes, and no data were excluded from the analyses.

Extended Data

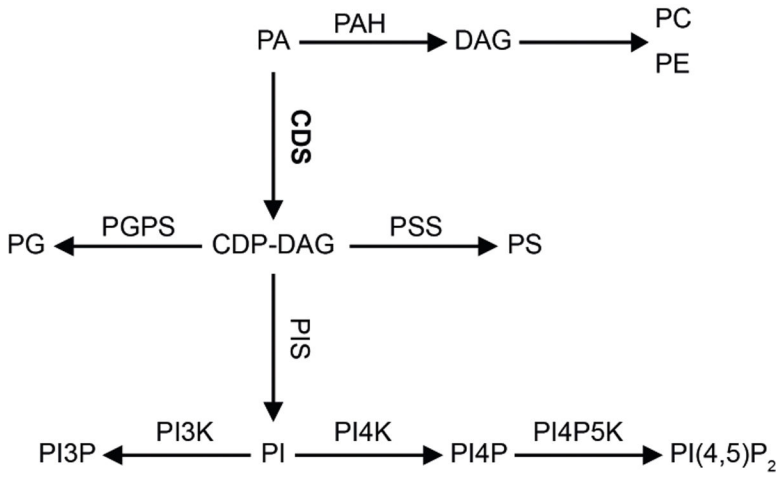

Extended Data Fig. 1 |. The plant glycerolipid metabolic pathway related to cytidinediphosphate-diacylglycerol synthase 1 (CDS1).

Rice RBL1 is homologous to yeast Cds1. CDP-DAG, cytidinediphosphate-diacylglycerol; DAG, diacylglycerol; PA, phosphatidic acid; PAH, phosphatidic acid phosphohydrolase; PC, phosphatidylcholine; PE, phosphatidylethanolamine; PG, phosphatidylglycerol; PGPS, phosphatidylglycerol phosphate synthase; PI, phosphatidylinositol; PI4K, phosphatidylinositol 4-kinases; PI4P, phosphatidylinositol 4-phosphate; PI4P5K, phosphatidylinositol 4-phosphate 5-kinase; $PI(4,5)P_2$, phosphatidylinositol-4,5-bisphosphate; PIS, phosphatidylinositol synthase; PS, phosphatidylserine; PSS, phosphatidylserine synthase.

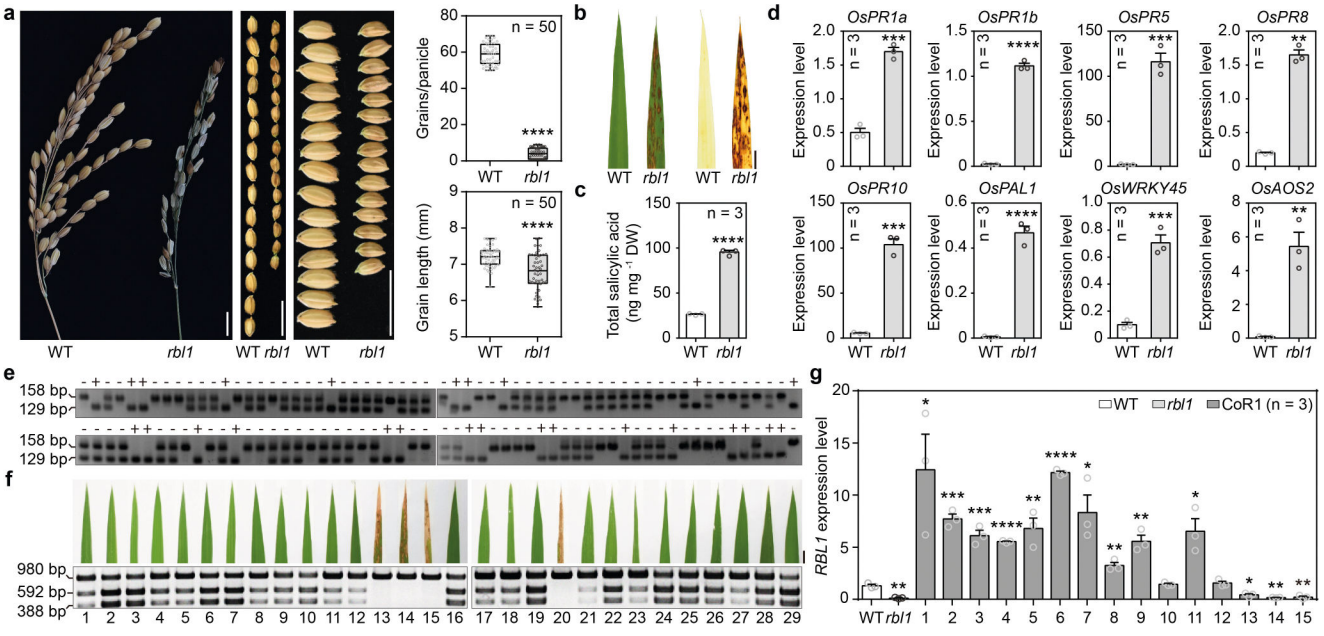

Extended Data Fig. 2 |. Expression of plant defense-related genes, yield, and genetic complementation of the *rbl1* line.

a, Panicles and seeds of the *rbl1* and WT lines. Bars, 1 cm. Grain yield of the *rbl1* and WT lines. Data are displayed as box and whisker plots with individual data points. The box plot elements are: center line, median; box limits, 25th and 75th percentiles. **b**, *In situ* detection of reactive oxygen species (ROS) in the *rbl1* mutant and wild-type (WT, KitaakeX) leaves using 3,3′-diaminobenzidine (DAB) staining. Bar, 1 cm. **c**, Total salicylic acid (SA) levels are increased in the *rbl1* mutant. Total SA was isolated from leaves of 2-week-old seedlings. **d**, qRT-PCR assays of genes that serve as markers of the plant immune response. Total RNA was extracted from leaves of 4-week-old plants. The *Actin* gene was used as the internal control. **e**, A 29 nucleotide deletion cosegregates with a lesion mimic phenotype in the M3 population derived from line *rbl1*. PCR results of InDel markers targeting the 29 nucleotide deletion: one short band, homozygous; one large band, wild-type alleles; two bands, heterozygous. "+" indicates lesions on the leaf of the M3 plant and "−" no lesion. A $\chi 2$ test of the phenotypic ratio revealed that the actual value 26: 92 of lesioned plants to normal plants is statistically similar to the expected value 1: 3 ($\chi 2 = 0.213$, P-value = 0.644 > 0.05). Similar results were obtained from three independent experiments. **f**, Complementation assays. Genotyping of the T0 lines using Cleaved Amplified Polymorphic Sequences (CAPS) markers. Leaves were photographed at 21 days post sowing (dps). For results of agarose gel electrophoresis, one band indicates the *rbl1* mutant and three bands indicate the complemented line. Bar, 1 cm. Similar results were obtained from three independent experiments. **g**, qRT-PCR assays of *RBL1* in the WT, *rbl1*, and complementation lines. Complementation line 10 was used as CoR1 in Fig. 1. The *Actin* gene was used as the internal control. Data are mean ± s.e.m, n = number of biologically independent samples in the graphs. Asterisks indicate significant differences compared to the WT using the two-tailed Student's *t*-test (**P* < 0.05, ***P* < 0.01, ****P* < 0.001, *****P* < 0.0001). For exact *P* values, see.

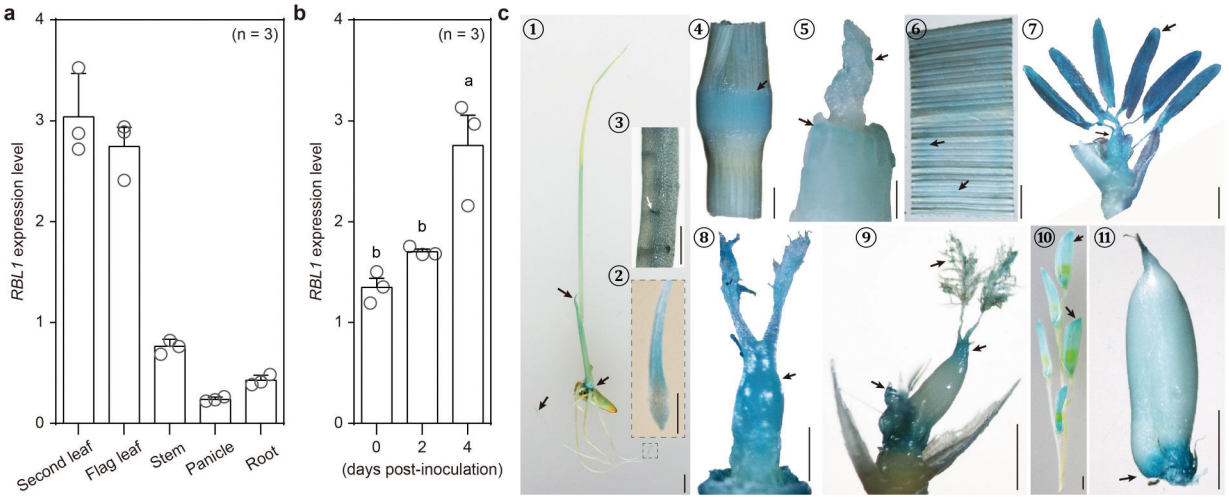

Extended Data Fig. 3 |. Expression assays of *RBL1*.

a, qRT-PCR assays of *RBL1* in different tissues of the wild-type (WT, Kitaake) plants at the flowering stage. **b**, qRT-PCR assays of *RBL1* in response to spray inoculation of *M. oryzae* strain ZB25 on Kitaake seedlings. **c**, Tissue-specific expression of *RBL1* visualized by staining for the β-glucuronidase (GUS) reporter activity under control of the *RBL1*

promoter. For numbers: 1, seedling; 2 and 3, root; 4, stem; 5, shoot apical mristem; 6, leaf; 7, stamen; 8, pistil; 9, premilk stage; 10, panicle; 11, maturity stage. Bars in 1, 4, and 7, 5 mm; bars in 2, 3, 5, 6, and 8 to 11, 1 mm. Data are mean ± s.e.m, n = number of biologically independent samples in the graphs. Significant differences indicated by different letters were calculated using the Duncan's new multiple range test.

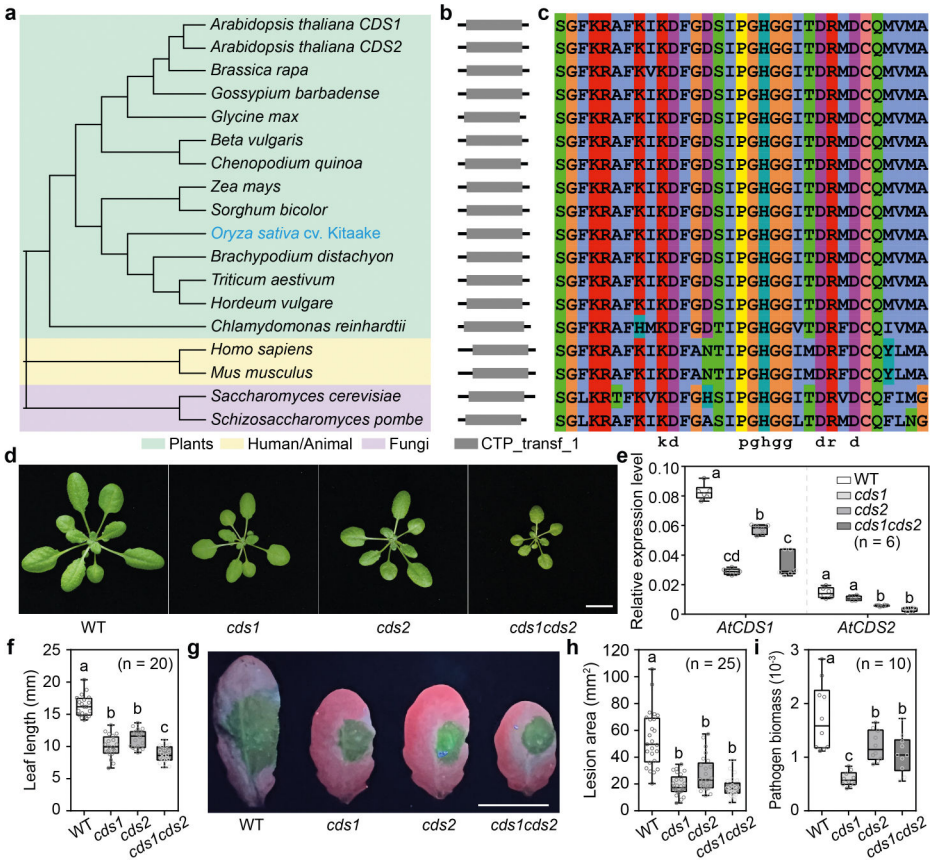

Extended Data Fig. 4 |. *Arabidopsis thaliana cds* mutants show enhanced resistance to *Phytophthora capsica*.

a, Phylogenetic analysis of RBL1 homologs from plants and other organisms. The phylogenetic tree was constructed using MEGA10. Accession numbers for different RBL1 homologs: *Arabidopsis thaliana* (NP_176433.2), *Beta vulgaris subsp. vulgaris* (XP_010694835.1), *Brachypodium distachyon* (XP_003564318.1), *Brassica rapa* (RID78417.1), *Chenopodium quinoa* (XP_021731901.1), *Chlamydomonas reinhardtii* (PNW85433.1), *Glycine max* (XP_003556374.1), *Gossypium barbadense* (KAB2026876.1), *Homo sapiens* (NP_001254.2), *Hordeum vulgare* (KAE8818711.1), *Mus musculus* (NP_775546.2), *Oryza sativa* (NC_029256.1), *Saccharomyces cerevisiae* (AJQ02739.1), *Schizosaccharomyces pombe* (NP_596416.1), *Sorghum bicolor* (KAG0539475.1), *Triticum aestivum* (KAF7023922.1), and *Zea mays* (NP_001132909.1). **b**, Protein domain analysis of RBL1 homologs from various organisms. Conserved protein domains in RBL1 homologs were predicted using SMART and visualized using iTOL. CTP_transf_1, phosphatide cytidylyltransferase. **c**, Amino acid alignment of the 19 residues that are truncated in the *rbl1* line. The consensus is shown at the bottom. **d**, The *cds* mutant and wild-type (WT, Col-0, *A.*

thaliana) plants at 28 days post sowing (dps). Bar, 1 cm. **e**, qRT-PCR assays. Total RNA was extracted from leaves of 4-week-old plants. **f**, Leaf length of the WT and *cds* mutant lines at 28 dps. **g**–**i**, Infected leaves (**g**), lesion area (**h**), and relative quantification of pathogen biomass (**i**) of WT and *cds* lines 36 h after inoculation (hpi) with *Phytophthora capsica* strain LT263. Bar, 1 cm. Data are mean ± s.e.m, n = number of biologically independent samples in the graphs. The box plot elements are: center line, median; box limits, 25th and 75th percentiles. Significant differences indicated by different letters were calculated using the Duncan's new multiple range test.

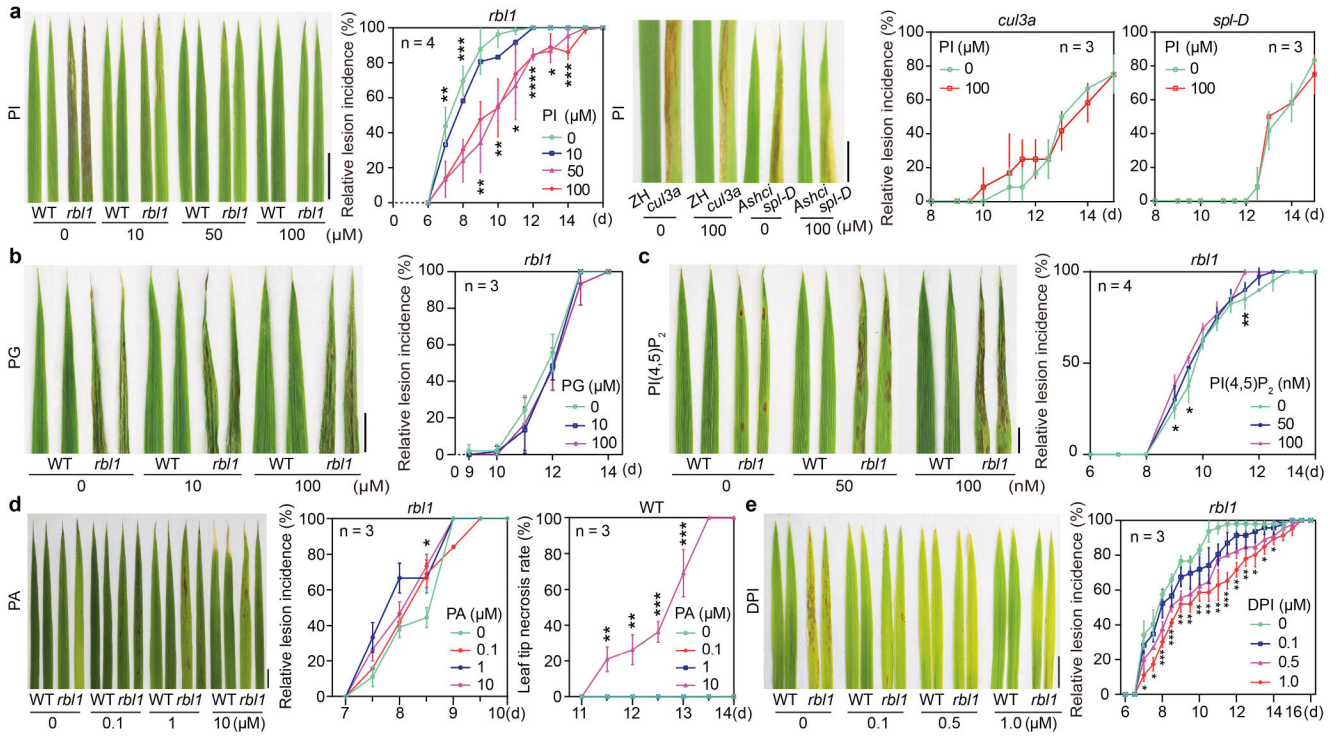

Extended Data Fig. 5 |. Exogenous supplementation of PI delays lesion formation in *rbl1*.
a, Lesion formation was suppressed in the *rbl1* but not *cul3a* or *spl-D* mutants. Plants were grown on 1/2 MS media supplemented with PI. WT, the wild-type Kitaake. Photographs were taken from 12-day-old *rbl1*, 2-week-old *clu3a*, and 2-week-old *spl-D* plants with corresponding control lines. Bar, 1 cm. **b**, Lesion formation in the *rbl1* mutant was not affected by application of exogenous PG. Plants were grown on the 1/2 MS media supplemented with PG. Photographs were taken from 12-day-old plants. Bar, 1 cm. **c**, Lesion formation in the *rbl1* mutant was enhanced with exogenous application of PI(4,5)P_2. Plants were grown on the 1/2 MS media supplemented with PI(4,5)P_2. Photographs were taken from 10-day-old plants. Bar, 1 cm. **d**, Exogenous PA enhances lesion formation in *rbl1* and leaf tip necrosis in WT. Bar, 1 cm. **e**, Lesion formation in *rbl1* was suppressed by exogenous diphenyleneiodonium chloride (DPI). Plants were grown on 1/2 MS media supplemented with DPI. Photographs were taken of 10-day-old plants. Bar, 1 cm. Data are mean ± s.e.m, n = number of independent replicates. Asterisks indicate significant differences compared to the mock using the two-tailed Student's *t*-test (*$P < 0.05$, **$P < 0.01$, ***$P < 0.001$, ****$P < 0.0001$). For exact P values, see.

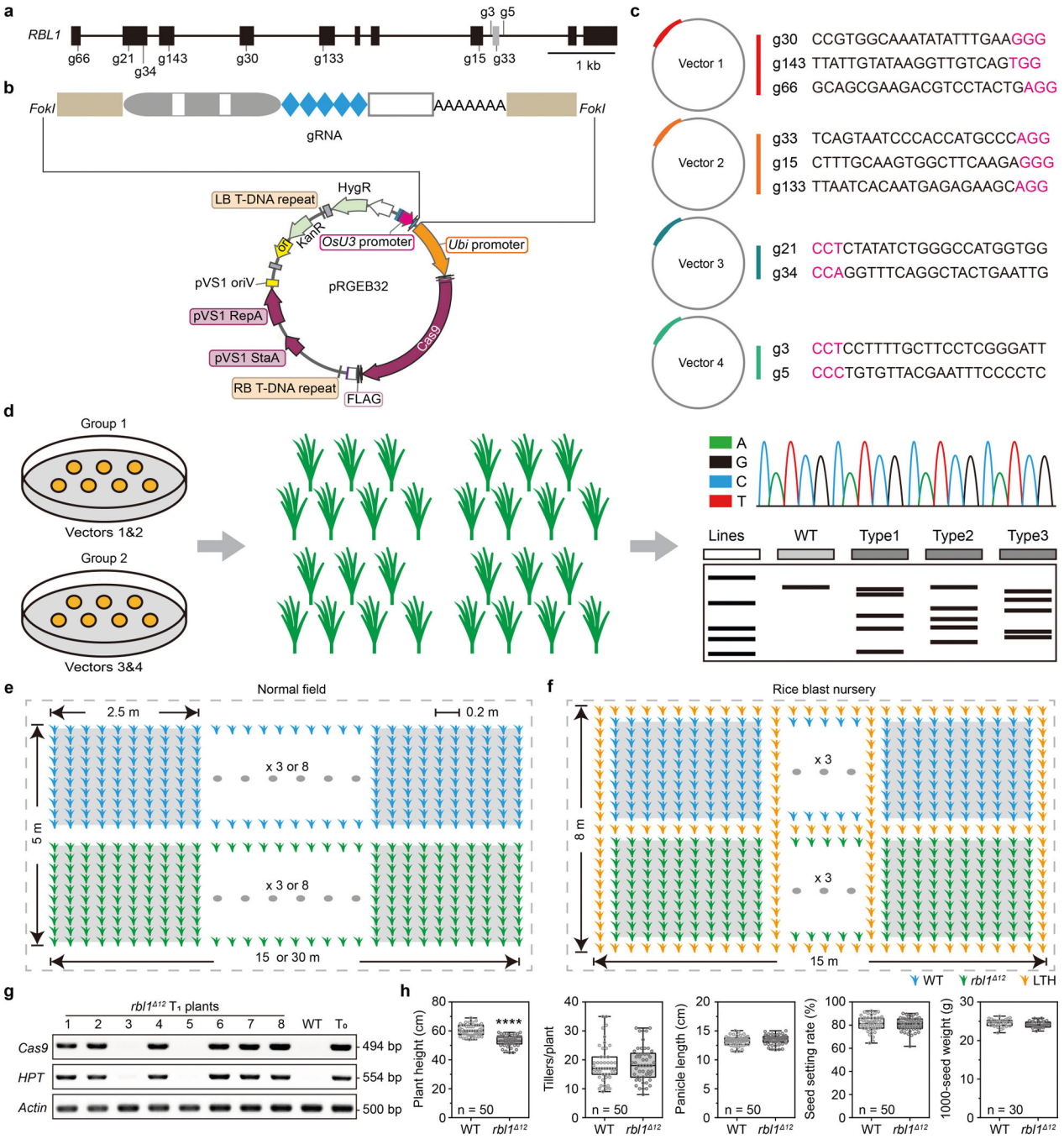

Extended Data Fig. 6 |. Design of multiplexed gRNAs for genome editing of *RBL1* and field trials.
a, Gene structure of *RBL1* and the site targeted by each numbered guide RNA (gRNA). **b**, Map and cloning sites of the CRISPR/Cas9 vector pRGEB32 used in genome editing (left); vectors with different gRNAs (right). **c**, Sequences of gRNAs designed using CRISPR-P 2.0. Purple letters indicate protospacer-adjacent motif sites (PAMs). **d**, A schematic diagram of co-transformation of different constructs and genotyping of T0 lines. Edited sites in each T0 plant were identified using Sanger sequencing and agarose gel electrophoresis. WT, the wild-type Kitaake. **e**, Design of the normal field plots. **f**, Design of the field plots in the rice

blast nursery. WT, the wild-type Kitaake; *rbl1*$^{\Delta 12}$, the edited line; LTH, the very susceptible rice variety Lijiangxintuanheigu, which was used as the spreader line for rice blast. Each plot contains 100 plants 0.2 m apart. **g**, Identification of transgene-free T1 plants of *rbl1*$^{\Delta 12}$. Primers specific to the *Cas9*, *hph* and *Actin* genes, respectively, were used in genotyping. The *hph* gene encoding a hygromycin B phosphotransferase confers hygromycin resistance in the rice transgenic lines. The amplicon of the *Actin* gene was used as the DNA quality control. WT, Kitaake. Similar results were obtained from three independent experiments. **h**. Agronomic traits of the *rbl1*$^{\Delta 12}$ and Kitaake lines. Data for each agronomic trait were collected from 50 plants for each line that was grown in the normal paddy field. Data are mean ± s.e.m, n = number of biologically independent samples in the graphs. In the box and whisker plots, dots indicate individual data points, and the error bars represent maximum and minimum values. Center line, median; box limits, 25th and 75th percentiles. Asterisks indicate significant differences using the two-tailed Student's *t*-test (****$P < 0.0001$). For exact *P* values, see.

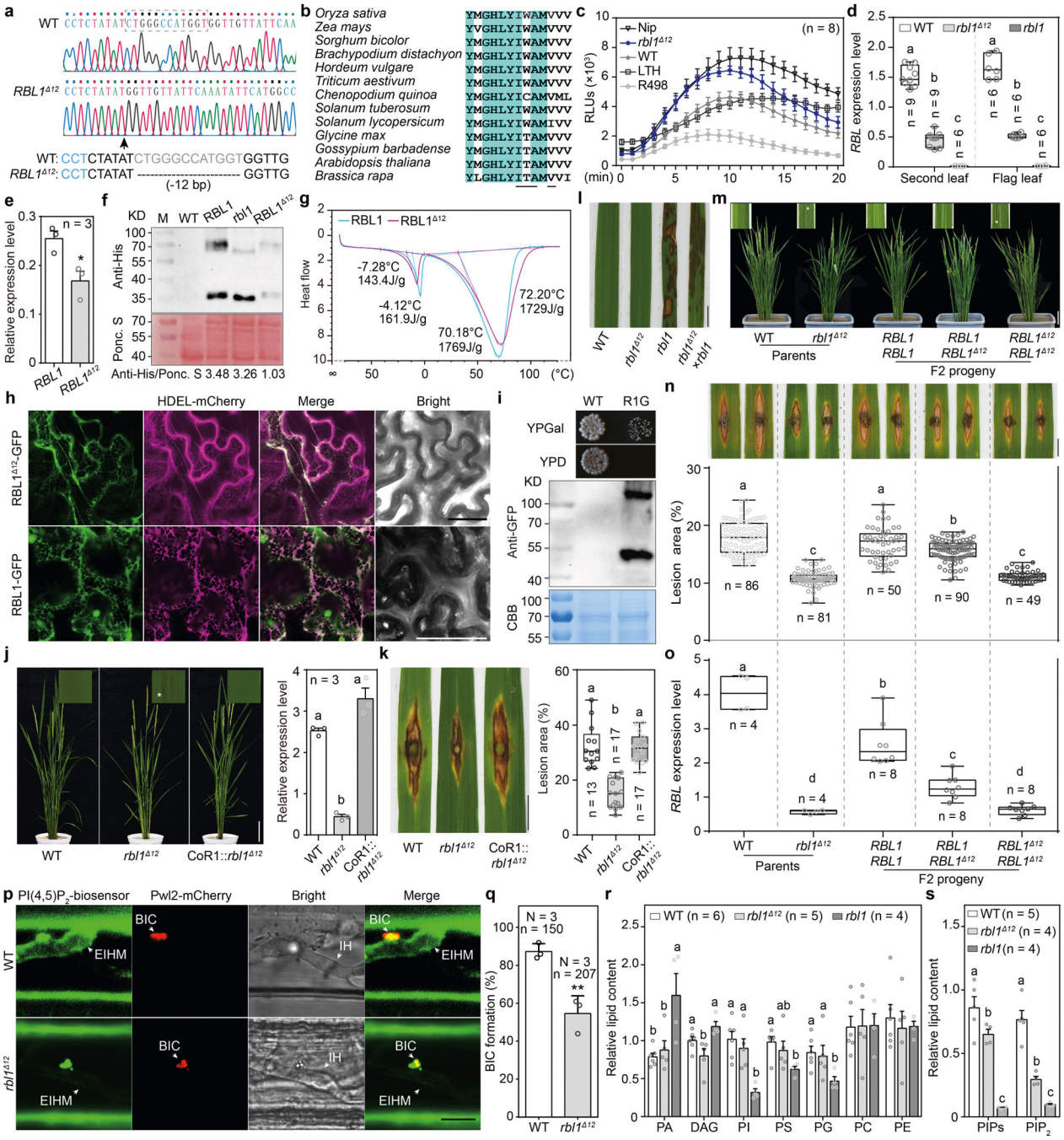

Extended Data Fig. 7 |. Characterization of the *rbl1*$^{\Delta 12}$ line and the allele.

a, Sanger sequencing of the edited site indicated by the arrow in the *rbl1*$^{\Delta 12}$ line with the wild-type (WT, Kitaake) as the reference. The PAM site was shown in blue, and the dashed line represents the 12 nucleotide deletion. **b**, Amino acid sequence alignment of RBL1 homologs around the four residues (underlined) that are truncated in the *rbl1*$^{\Delta 12}$ line. Highlighted are conserved residues in the RBL1 homologs. **c**, ROS generation in the WT, *rbl1*$^{\Delta 12}$, Nipponbare (Nip), LTH, and R498 rice plants challenged with chitin at the booting stage. RLU, relative light unit. **d**, qRT-PCR assays of *RBL1* expression in different

tissues of the WT, *rbl1*$^{\Delta 12}$, and *rbl1* plants at the flowering stage. **e**, qRT-PCR assays of heterologous expression of *RBL1* in yeast. Yeast 18s rRNA was used as the internal control. **f**, Immunoblotting analysis of RBL1-, rbl1-, and RBL1$^{\Delta 12}$-6×His fusion proteins in yeast. Ponceau S staining indicates the protein loading. WT, yeast strain BY4741; other strains are transformants of the yeast *cds1* mutant carrying pYES2-*RBL1*, pYES2-*rbl1*, and pYES2- *RBL1*$^{\Delta 12}$, respectively. Similar results were obtained from three independent experiments. **g**, Stability of the RBL1- and RBL1$^{\Delta 12}$-6×His fusion proteins analyzed using differential scanning calorimetry (DSC). **h**, Subcellular localization of the RBL1- and RBL1$^{\Delta 12}$-GFP fusion proteins transiently expressed in *Nicotiana benthamiana* leaf epidermal cells, analyzed together with the endoplasmic reticulum marker HDEL-mCherry. Bars, 25 μm. **i**, RBL1-GFP rescues the growth defect of yeast *cds1*. WT, yeast strain BY4741; R1G, the yeast *cds1* mutant carrying pYES2-*RBL1*-GFP. Strains were cultured on YPGal or YPD plates at 30 °C for 3 days before sampling. Immunoblotting analysis of the RBL1-GFP fusion protein in the yeast strain R1G that forms a homodimer. CBB staining indicates the protein loading. Similar results were obtained from three independent experiments. **j**, 9-week-old WT, *rbl1*$^{\Delta 12}$, and complemented T1 plants. The white asterisk indicates the spontaneous lesion in the insets. Bar, 10 cm. Shown on the right are qRT-PCR assays of *RBL1* in the WT, *rbl1*$^{\Delta 12}$, and CoR1:: *rbl1*$^{\Delta 12}$ lines. The *Actin* gene was used as the internal control. **k**, Punch inoculation of the WT, *rbl1*$^{\Delta 12}$, and CoR1:: *rbl1*$^{\Delta 12}$ lines with *M. oryzae*. The lesion area was measured at 14 dpi. Bar, 1 cm. **l**, Leaves of 3-week-old WT, *rbl1*, *rbl1*$^{\Delta 12}$, and F1 plants of *rbl1* crossed with *rbl1*$^{\Delta 12}$. Bar, 1 cm. **m**, The WT, *rbl1*$^{\Delta 12}$, and F2 plants derived from the WT line crossed with *rbl1*$^{\Delta 12}$ at 60 dps. Spontaneous lesions-indicated by white asterisks-formed on the top leaves of homozygous *rbl1*$^{\Delta 12}$ lines. Bars, 10 cm. **n**, Punch inoculation assays of the WT, *rbl1*$^{\Delta 12}$, and F2 plants with *M. oryzae*. The lesion area was measured at 14 dpi. Bar, 1 cm. **o**, qRT-PCR assays of *RBL1* in the WT, *rbl1*$^{\Delta 12}$ and F2 plants at the tillering stage. **p**, WT and *rbl1*$^{\Delta 12}$ transgenic plants expressing the PI(4,5)P_2 biosensor at 32 hpi with *M. oryzae* stain ZB25 expressing the cytoplasmic effector Pwl2 tagged with mCherry. BIC, biotrophic interfacial complex; EIHM, extra-invasive hyphal membrane; IH, invasive hyphae. Bar, 10 μm. **q**, BIC formation in plants shown in (**p**). **r**, Membrane lipid composition analysis of the WT, *rbl1*$^{\Delta 12}$, and *rbl1* lines. DW, dry weight. **s**, PIP and PIP_2 content in the WT, *rbl1*$^{\Delta 12}$, and *rbl1* lines. Data are mean ± s.e.m, n = number of biologically independent samples in the graphs. The box plot elements are: center line, median; box limits, 25th and 75th percentiles. Asterisks in (**e**) and (**q**) indicate significant differences using the two-tailed Student's *t*-test (*$P < 0.05$, **$P < 0.01$). For exact *P* values, see Source Data. Significant differences indicated by different letters in (**d**),(**j**),(**k**), (**n**),(**o**),(**r**), and (**s**) were calculated using the Duncan's new multiple range test.

Extended Data Fig. 8 |. No mutations were observed in predicted off-target sites in *rbl1*$^{\Delta 12}$. The top seven predicted off-target sites were analyzed using Sanger sequencing with the Kitaake (WT) genome as the reference. Purple letters indicate protospacer-adjacent motif sites (PAMs). The right panel shows the sequencing results of the potential off-target sites.

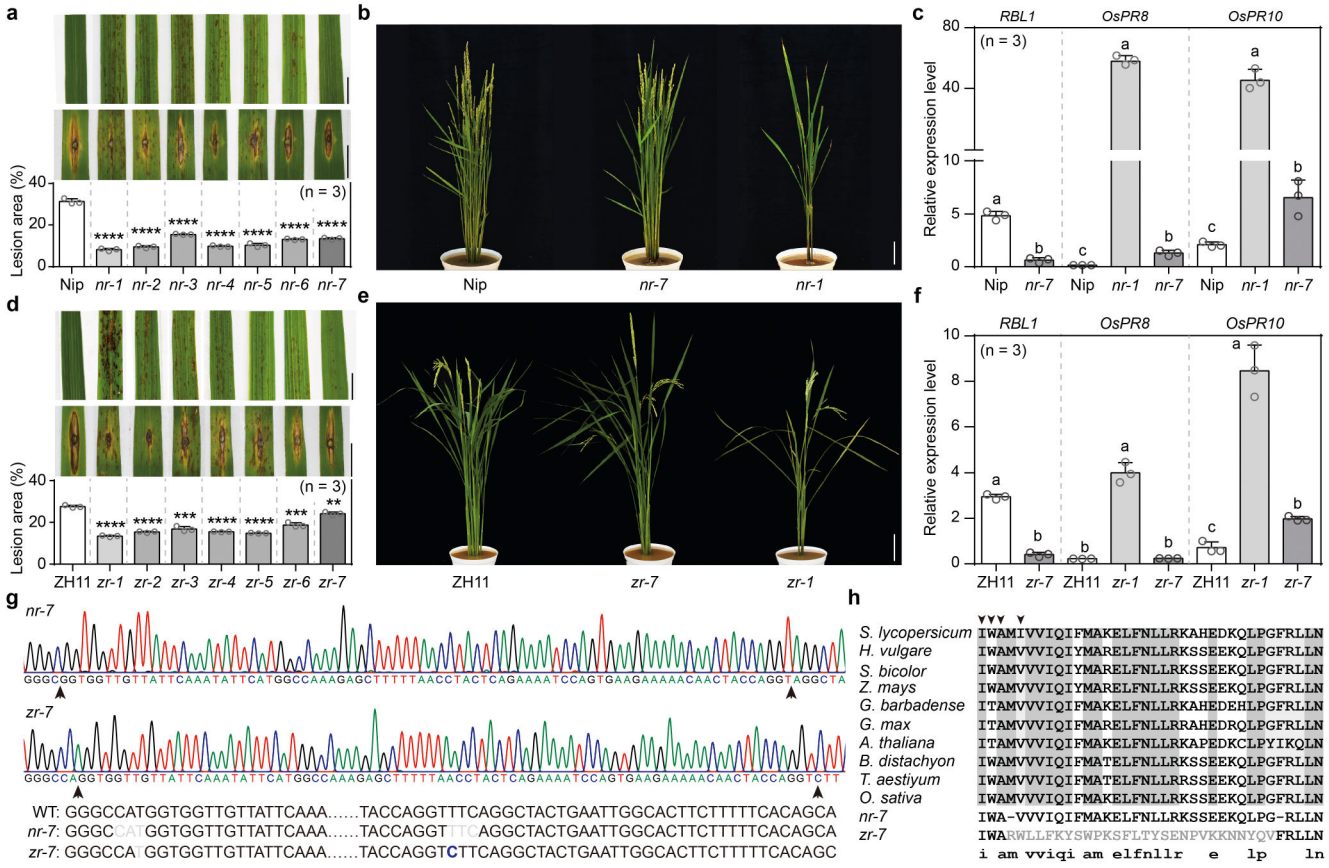

Extended Data Fig. 9 |. Genome editing of *RBL1* enhances disease resistance in two other rice cultivars.

a, Lesion mimic phenotypes and enhanced resistance to *M. oryzae* in *RBL1*-edited Nipponbare (Nip) lines. Infected leaves and lesion area of punch-inoculated *RBL1*-edited lines with *M. oryzae* at 14 dpi. Bar, 1 cm. **b**, 12-week-old *RBL1*-edited Nipponbare lines. Bar, 10 cm. **c**, qRT-PCR assays of *RBL1* and plant defense-related genes *OsPR8* and *OsPR10* in the *RBL1*-edited Nipponbare lines. Total RNA was extracted from 4-week-old leaves. The *Actin* gene was used as the internal control. **d**–**f**, Similar assays as shown in (**a**–**c**) were performed on rice cultivar Zhonghua11 (ZH11). **g**, Sanger sequencing of the edited sites, indicated by arrows, in *nr-7* and *zr-7* lines, with the wild-type (WT, Kitaake) as the reference. The mutated nucleotides are shown in gray (deletion) and blue (insertion). **h**, Amino acid sequence alignment of the region mutated in lines *nr-7* and *zr-7*. The four amino acids truncated in $RBL1^{\Delta 12}$ are indicated by arrows. Shaded are conserved residues in the RBL1 homologs. Two amino acids are truncated in *nr-7*, with the first one overlapping the truncated residues in $RBL1^{\Delta 12}$. An 84-bp frameshift mutation caused by a 1-bp deletion followed by a 1-bp insertion alters the sequence of 28 amino acids (gray) in *zr-7*, with the first two overlapping the truncated residues in $RBL1^{\Delta 12}$. Data are mean ± s.e.m, n = number of biologically independent samples in the graphs. And asterisks indicate significant differences compared to the WT using the unpaired Student's *t*-test (** $P < 0.01$, *** $P < 0.001$, **** $P < 0.0001$). For exact *P* values, see Source Data. Significant differences indicated by different letters in (**c**) and (**f**) were calculated using the Duncan's new multiple range test.

Supplementary Material

Refer to Web version on PubMed Central for supplementary material.

Acknowledgements

We thank G. Wang and Y. Ning for the pRGV and pRHV vectors; X. Chen and D. Dou for the *M. oryzae* and *P. capsici* strains, respectively; Z. Wang for the Pwl2– mCherry marker; W. Zhao and L. Cao for the rice *spl-D* and *cul3a* mutants, respectively; H. Xue for the *Arabidopsis cds* mutants; P. Fei for technical support with confocal imaging; and G. Ren for the field trials; H. Hu for the pEarleyGate101 vector and HDEL–mCherry markers; D. Duanmu for the pYES2–NTA vectors; W. Chen for the total salicylic acid analysis; C. Luo, M. Yuan and Z. Lai for the *U. virens*, *Xoo* strains and *Arabidopsis* lines; Z. Hu and X. Shen for their support with data acquisition and analysis; and J. Zhou, X. Chen, H. He, X. Wang and J. R. Xu for discussions. The phospholipid analysis was performed on the lipidomics platform of the National Key Laboratory of Crop Genetic Improvement. Confocal laser scanning microscope data were acquired at the National Key Laboratory of Agricultural Microbiology Core Facility. The computations in this paper were run on the bioinformatics computing platform of the National Key Laboratory of Crop Genetic Improvement. This work was supported by the National Key R&D Program of China (2022YFA1304402), Natural Science Foundation of China (32172373 and 31801723), Fundamental Research Funds for the Central Universities (2662020ZKPY006, 2023ZKPY002 and 2662023PY006) and the Open Research Fund of the State Key Laboratory of Hybrid Rice (Wuhan University) (KF202202) to G.L. J.C.M. is supported by the Joint Bioenergy Institute funded by the US Department of Energy (DE-AC02–05CH11231). The phospholipid measurements were performed with support from the Bordeaux Metabolome Facility-MetaboHUB (ANR-11-INBS-0010) and Fundamental Research Funds for the Central Universities (2662020ZKPY005). Research in the Ronald Laboratory was supported by the National Science Foundation, the National Institutes of Health (GM122968 and GM55962) and the Joint Bioenergy Institute funded by the US Department of Energy (DE-AC02–05CH11231).

Data availability

Sequencing data for the pooled M_3 plants derived from the *rbl1* line (FN398) are available at the National Center for Biotechnology Information under the accession number

SRR4096918. Other sequences can be accessed under the following numbers: *RBL1* (LOC_Os01g55360, NP_001044302.1), *OsPIS1* (LOC_Os02g03110, NC_029257.1) and *OsPAH2* (LOC_Os11g40080, XP_015617116.1). Original data points in graphs are shown in the source data files. Uncropped gel and immunoblotting images can be found in Supplementary Fig. 1. All plasmids and plant lines generated in this work are available from the authors upon request. Source data are provided with this paper.

References

1. Gao C Genome engineering for crop improvement and future agriculture. Cell 184, 1621–1635 (2021). [PubMed: 33581057]
2. Liu X, Yin Y, Wu J & Liu Z Structure and mechanism of an intramembrane liponucleotide synthetase central for phospholipid biosynthesis. Nat. Commun. 5, 4244 (2014). [PubMed: 24968740]
3. Qin L et al. Specific recruitment of phosphoinositide species to the plant–pathogen interfacial membrane underlies *Arabidopsis* susceptibility to fungal infection. Plant Cell 32, 1665–1688 (2020). [PubMed: 32156686]
4. Zhu H, Li C & Gao C Applications of CRISPR–Cas in agriculture and plant biotechnology. Nat. Rev. Mol. Cell Biol. 21, 661–677 (2020). [PubMed: 32973356]
5. Chen K, Wang Y, Zhang R, Zhang H & Gao C CRISPR/Cas genome editing and precision plant breeding in agriculture. Annu. Rev. Plant Biol. 70, 667–697 (2019). [PubMed: 30835493]
6. Sakulkoo W et al. A single fungal MAP kinase controls plant cell-to-cell invasion by the rice blast fungus. Science 359, 1399–1403 (2018). [PubMed: 29567712]
7. Li W, Chern M, Yin J, Wang J & Chen X Recent advances in broad-spectrum resistance to the rice blast disease. Curr. Opin. Plant Biol. 50, 114–120 (2019). [PubMed: 31163394]
8. Song W-Y et al. A receptor kinase-like protein encoded by the rice disease resistance gene, *Xa21*. Science 270, 1804–1806 (1995). [PubMed: 8525370]
9. Li W et al. A natural allele of a transcription factor in rice confers broad-spectrum blast resistance. Cell 170, 114–126 (2017). [PubMed: 28666113]
10. Deng Y et al. Epigenetic regulation of antagonistic receptors confers rice blast resistance with yield balance. Science 355, 962–965 (2017). [PubMed: 28154240]
11. Wang J et al. A single transcription factor promotes both yield and immunity in rice. Science 361, 1026–1028 (2018). [PubMed: 30190406]
12. Gao M et al. Ca^{2+} sensor-mediated ROS scavenging suppresses rice immunity and is exploited by a fungal effector. Cell 184, 5391–5404 (2021). [PubMed: 34597584]
13. Hu X-H et al. A natural allele of proteasome maturation factor improves rice resistance to multiple pathogens. Nat. Plants 9, 228–237 (2023). [PubMed: 36646829]
14. Krattinger SG et al. A putative ABC transporter confers durable resistance to multiple fungal pathogens in wheat. Science 323, 1360–1363 (2009). [PubMed: 19229000]
15. Wang N et al. Inactivation of a wheat protein kinase gene confers broad-spectrum resistance to rust fungi. Cell 185, 2961–2974 (2022). [PubMed: 35839760]
16. Büschges R et al. The barley *Mlo* gene: a novel control element of plant pathogen resistance. Cell 88, 695–705 (1997). [PubMed: 9054509]
17. Li S et al. Genome-edited powdery mildew resistance in wheat without growth penalties. Nature 602, 455–460 (2022). [PubMed: 35140403]
18. Lorrain S, Vailleau F, Balagué C & Roby D Lesion mimic mutants: keys for deciphering cell death and defense pathways in plants?. Trends Plant Sci. 8, 263–271 (2003). [PubMed: 12818660]
19. Xing J, Zhang L, Duan Z & Lin J Coordination of phospholipid-based signaling and membrane trafficking in plant immunity. Trends Plant Sci. 26, 407–420 (2021). [PubMed: 33309101]
20. Liu L, Waters DLE, Rose TJ, Bao J & King GJ Phospholipids in rice: significance in grain quality and health benefits: a review. Food Chem. 139, 1133–1145 (2013). [PubMed: 23561219]

21. Shimada TL et al. Enrichment of phosphatidylinositol 4,5-bisphosphate in the extra-invasive hyphal membrane promotes colletotrichum infection of *Arabidopsis thaliana*. Plant Cell Physiol. 60, 1514–1524 (2019). [PubMed: 30989198]
22. Li G et al. The sequences of 1504 mutants in the model rice variety Kitaake facilitate rapid functional genomic studies. Plant Cell 29, 1218–1231 (2017). [PubMed: 28576844]
23. You Q et al. An E3 ubiquitin ligase-BAG protein module controls plant innate immunity and broad-spectrum disease resistance. Cell Host Microbe 20, 758–769 (2016). [PubMed: 27978435]
24. Zhao X et al. A novel glycine-rich domain protein, GRDP1, functions as a critical feedback regulator for controlling cell death and disease resistance in rice. J. Exp. Bot. 72, 608–622 (2021). [PubMed: 32995857]
25. Liu Q et al. OsCUL3a negatively regulates cell death and immunity by degrading OsNPR1 in rice. Plant Cell 29, 345–359 (2017). [PubMed: 28100706]
26. Zhou Y et al. Extraplastidial cytidinediphosphate diacylglycerol synthase activity is required for vegetative development in *Arabidopsis thaliana*. Plant J. 75, 867–879 (2013). [PubMed: 23711240]
27. Blunsom NJ & Cockcroft S CDP-diacylglycerol synthases (CDS): gateway to phosphatidylinositol and cardiolipin synthesis. Front. Cell Dev. Biol. 8, 63 (2020). [PubMed: 32117988]
28. Li J & Wang X Phospholipase D and phosphatidic acid in plant immunity. Plant Sci. 279, 45–50 (2019). [PubMed: 30709492]
29. Khang CH et al. Translocation of *Magnaporthe oryzae* effectors into rice cells and their subsequent cell-to-cell movement. Plant Cell 22, 1388–1403 (2010). [PubMed: 20435900]
30. Du XQ, Yao HY, Luo P, Tang XC & Xue HW Cytidinediphosphate diacylglycerol synthase —mediated phosphatidic acid metabolism is crucial for early embryonic development of *Arabidopsis*. PLoS Genet. 18, e1010320 (2022). [PubMed: 35877676]
31. Hong Y, Yuan S, Sun L, Wang X & Hong Y Cytidinediphosphate-diacylglycerol synthase 5 is required for phospholipid homeostasis and is negatively involved in hyperosmotic stress tolerance. Plant J. 94, 1038–1050 (2018). [PubMed: 29604140]
32. Di Paolo G & De Camilli P Phosphoinositides in cell regulation and membrane dynamics. Nature 443, 651–657 (2006). [PubMed: 17035995]
33. Kale SD et al. External lipid PI3P mediates entry of eukaryotic pathogen effectors into plant and animal host cells. Cell 142, 284–295 (2010); erratum 142, 981–983 (2010). [PubMed: 20655469]
34. Liu L et al. The *Xanthomonas* type III effector XopAP prevents stomatal closure by interfering with vacuolar acidification. J. Integr. Plant Biol. 64, 1994–2008 (2022). [PubMed: 35972796]
35. Wang H et al. A plant virus hijacks phosphatidylinositol-3,5-bisphosphate to escape autophagic degradation in its insect vector. Autophagy 19, 1128–1143 (2023). [PubMed: 36093594]
36. Marković V & Jaillais Y Phosphatidylinositol 4-phosphate: a key determinant of plasma membrane identity and function in plants. New Phytol. 235, 867–874 (2022). [PubMed: 35586972]
37. Boni R et al. Pathogen-inducible *Ta-Lr34res* expression in heterologous barley confers disease resistance without negative pleiotropic effects. Plant Biotechnol. J. 16, 245–253 (2018). [PubMed: 28561994]
38. Gruner K et al. Evidence for allele-specific levels of enhanced susceptibility of wheat mlo mutants to the hemibiotrophic fungal pathogen Magnaporthe oryzae pv. Triticum. Genes 11, 517 (2020). [PubMed: 32392723]
39. Li W, Deng Y, Ning Y, He Z & Wang G-L Exploiting broad-spectrum disease resistance in crops: from molecular dissection to breeding. Annu. Rev. Plant Biol. 71, 575–603 (2020). [PubMed: 32197052]
40. Oliva R et al. Broad-spectrum resistance to bacterial blight in rice using genome editing. Nat. Biotechnol. 37, 1344–1350 (2019). [PubMed: 31659337]
41. Lu Y et al. Targeted, efficient sequence insertion and replacement in rice. Nat. Biotechnol. 38, 1402–1407 (2020). [PubMed: 32632302]
42. Li G et al. Genome-wide sequencing of 41 rice (Oryza sativa L.) mutated lines reveals diverse mutations induced by fast-neutron irradiation. Mol. Plant 9, 1078–1081 (2016). [PubMed: 27018389]
43. Jain R et al. Genome sequence of the model rice variety KitaakeX. BMC Genom. 20, 905 (2019).

44. Tang J et al. GDSL lipase occluded stomatal pore 1 is required for wax biosynthesis and stomatal cuticular ledge formation. New Phytol. 228, 1880–1896 (2020). [PubMed: 32542680]
45. Park C-J & Ronald PC Cleavage and nuclear localization of the rice XA21 immune receptor. Nat. Commun. 3, 920 (2012). [PubMed: 22735448]
46. Zhou X et al. Loss of function of a rice TPR-domain RNA-binding protein confers broad-spectrum disease resistance. Proc. Natl Acad. Sci. USA 115, 3174–3179 (2018). [PubMed: 29432165]
47. Li G et al. *MST50* is involved in multiple MAP kinase signaling pathways in *Magnaporthe oryzae*. Environ. Microbiol. 19, 1959–1974 (2017). [PubMed: 28244240]
48. Li GB et al. Overproduction of OsRACK1A, an effector-targeted scaffold protein promoting OsRBOHB-mediated ROS production, confers rice floral resistance to false smut disease without yield penalty. Mol. Plant 15, 1790–1806 (2022). [PubMed: 36245122]
49. Li Q et al. A Phytophthora capsici effector targets ACD11 binding partners that regulate ROS-mediated defense response in Arabidopsis. Mol. Plant 12, 565–581 (2019). [PubMed: 30703564]
50. DeZwaan TM, Carroll AM, Valent B & Sweigard JA *Magnaporthe grisea* Pth11p is a novel plasma membrane protein that mediates appressorium differentiation in response to inductive substrate cues. Plant Cell 11, 2013–2030 (1999). [PubMed: 10521529]
51. Jones K et al. Disruption of the interfacial membrane leads to *Magnaporthe oryzae* effector re-location and lifestyle switch during rice blast disease. Front. Cell Dev. Biol. 9, 681734 (2021). [PubMed: 34222251]
52. Chen X et al. An ATPase promotes autophosphorylation of the pattern recognition receptor XA21 and inhibits XA21-mediated immunity. Proc. Natl Acad. Sci. USA 107, 8029–8034 (2010). [PubMed: 20385831]
53. Luu DD et al. Biosynthesis and secretion of the microbial sulfated peptide RaxX and binding to the rice XA21 immune receptor. Proc. Natl Acad. Sci. USA 116, 8525–8534 (2019). [PubMed: 30948631]
54. Fan J et al. The monocot-specific receptor-like kinase SDS2 controls cell death and immunity in rice. Cell Host Microbe 23, 498–510 (2018). [PubMed: 29576481]
55. Chen X et al. The ‘pears and lemons’ protein UvPal1 regulates development and virulence of Ustilaginoidea virens. Environ. Microbiol. 22, 5414–5432 (2020). [PubMed: 33073491]
56. Fan J et al. The false smut pathogen *Ustilaginoidea virens* requires rice stamens for false smut ball formation. Environ. Microbiol. 22, 646–659 (2020). [PubMed: 31797523]
57. Livak KJ & Schmittgen TD Analysis of relative gene expression data using real-time quantitative PCR and the 2−ΔΔCT method. Methods 25, 402–408 (2001). [PubMed: 11846609]
58. Haselier A, Akbari H, Weth A, Baumgartner W & Frentzen M Two closely related genes of *Arabidopsis* encode plastidial cytidinediphosphate diacylglycerol synthases essential for photoautotrophic growth. Plant Physiol. 153, 1372–1384 (2010). [PubMed: 20442275]
59. Durowoju IB, Bhandal KS, Hu J, Carpick B & Kirkitadze M Differential scanning calorimetry — a method for assessing the thermal stability and conformation of protein antigen. J. Vis. Exp. 121, e55262 (2017).
60. Li Q et al. Understanding the biochemical basis of temperature-induced lipid pathway adjustments in plants. Plant Cell 27, 86–103 (2015). [PubMed: 25564555]
61. Lu S, Liu H, Jin C, Li Q & Guo L An efficient and comprehensive plant glycerolipids analysis approach based on high-performance liquid chromatography-quadrupole time-of-flight mass spectrometer. Plant Direct 3, e00183 (2019). [PubMed: 31832598]
62. Ito Y et al. Sphingolipids mediate polar sorting of PIN2 through phosphoinositide consumption at the *trans*-Golgi network. Nat. Commun. 12, 4267 (2021). [PubMed: 34257291]
63. He F, Zhang F, Sun W, Ning Y & Wang G-L A versatile vector toolkit for functional analysis of rice genes. Rice 11, 27 (2018). [PubMed: 29679176]
64. Santoni V Plant plasma membrane protein extraction and solubilization for proteomic analysis. Methods Mol. Biol 355, 93–109 (2007). [PubMed: 17093306]
65. Yang H et al. Pore architecture of TRIC channels and insights into their gating mechanism. Nature 538, 537–541 (2016). [PubMed: 27698420]

66. Colin L et al. Imaging the living plant cell: from probes to quantification. Plant Cell 34, 247–272 (2022). [PubMed: 34586412]

67. Tang N et al. MODD mediates deactivation and degradation of OsbZIP46 to negatively regulate ABA signaling and drought resistance in rice. Plant Cell 28, 2161–2177 (2016). [PubMed: 27468891]

68. Zhai K et al. NLRs guard metabolism to coordinate pattern- and effector-triggered immunity. Nature 601, 245–251 (2022). [PubMed: 34912119]

69. Gutteridge S & Gatenby AA Rubisco synthesis, assembly, mechanism, and regulation. Plant Cell 7, 809–819 (1995). [PubMed: 12242387]

70. Simon ML et al. A multi-colour/multi-affinity marker set to visualize phosphoinositide dynamics in *Arabidopsis*. Plant J. 77, 322–337 (2014). [PubMed: 24147788]

71. Xie K, Minkenberg B & Yang Y Boosting CRISPR/Cas9 multiplex editing capability with the endogenous tRNA-processing system. Proc. Natl Acad. Sci. USA 112, 3570–3575 (2015). [PubMed: 25733849]

72. Minkenberg B, Zhang J, Xie K & Yang Y CRISPR-PLANT v2: an online resource for highly specific guide RNA spacers based on improved off-target analysis. Plant Biotechnol. J. 17, 5–8 (2019). [PubMed: 30325102]

73. Xie X et al. CRISPR-GE: a convenient software toolkit for CRISPR-based genome editing. Mol. Plant 10, 1246–1249 (2017). [PubMed: 28624544]

74. IRRI. Standard Evaluation System for Rice (SES) 17–18 (International Rice Research Institute, 2002).

75. Yang L et al. The genome of the rice variety LTH provides insight into its universal susceptibility mechanism to worldwide rice blast fungal strains. Comput. Struct. Biotechnol. J. 20, 1012–1026 (2022). [PubMed: 35242291]

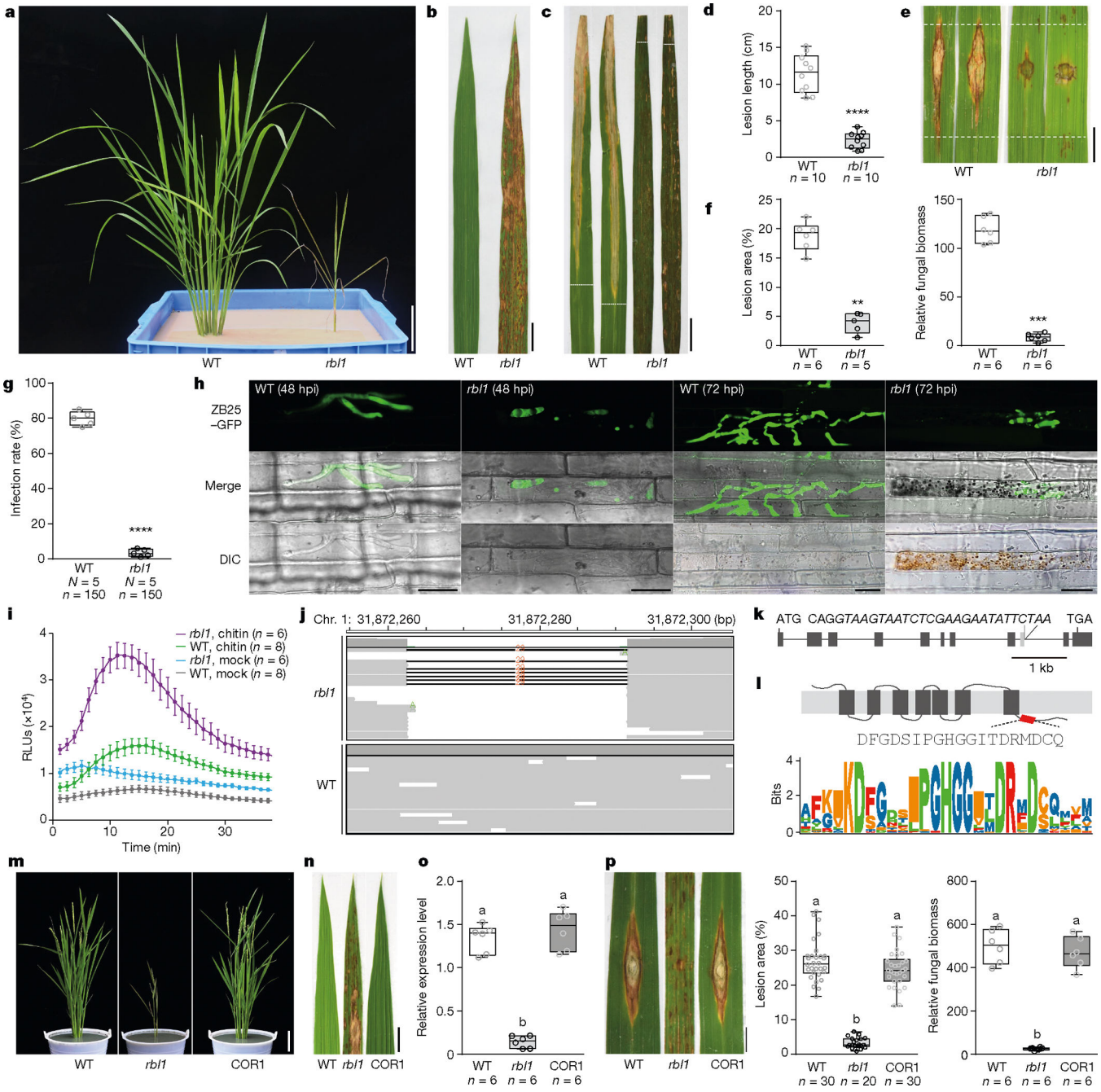

Fig. 1 |. Cloning the *RBL1* gene from the LMM *rbl1*, which has enhanced immunity.

a, Wild-type (WT, KitaakeX) and *rbl1* mutant plants at 40 days after sowing. Scale bar, 10 cm. **b**, Spontaneous lesions. Scale bar, 1 cm. **c**, Inoculation of rice lines with *Xoo* at 14 days post-inoculation (dpi). Scale bar, 1 cm. **d**, Lesion length at 14 dpi for WT and *rbl1* plants. **e**, Punch inoculation with *M. oryzae* at 14 dpi. The area between the dashed lines was covered by aluminium foil before spontaneous lesions appeared. Scale bar, 1 cm. **f**, Lesion area and relative fungal biomass. **g**, Fungal infection rates at 72 hpi. **h**, Rice sheath cells infected by eGFP-tagged *M. oryzae* strain ZB25. Scale bars, 25 μm. **i**, ROS generation in rice plants challenged with chitin and water (mock). RLU, relative light unit. **j**, Screenshot

of the 29 nucleotide deletion in *rbl1*. Chr., chromosome. **k**, Gene structure of *RBL1*. The grey box indicates the exon skipped in *rbl1*. The sequence of the deletion is shown and the intron sequence is in italic. **l**, Schematic diagram of RBL1. The red box indicates the truncation. The CDS signature motif is shown at the bottom. **m**, 10-week-old WT, *rbl1* and complemented (COR1) plants. Scale bar, 10 cm. COR1, *rbl1* complemented plants. **n**, Leaves of the lines shown in **m**. **o**, Quantitative PCR with reverse transcription (RT–qPCR) assays of *RBL1*. **p**, Infection assays with *M. oryzae* at 14 dpi. All data are mean ± s.e.m.; *n* is the number of biologically independent samples. Box plots with individual data points: centre line, median; box limits, 25th and 75th percentiles. Asterisks indicate significant differences using the two-tailed Student's *t*-test (***P* < 0.01, ****P* < 0.001, *****P* < 0.0001). For exact *P* values, see Source Data. Significant differences indicated by different letters (in **o** and **p**) were calculated using the Duncan's new multiple range test.

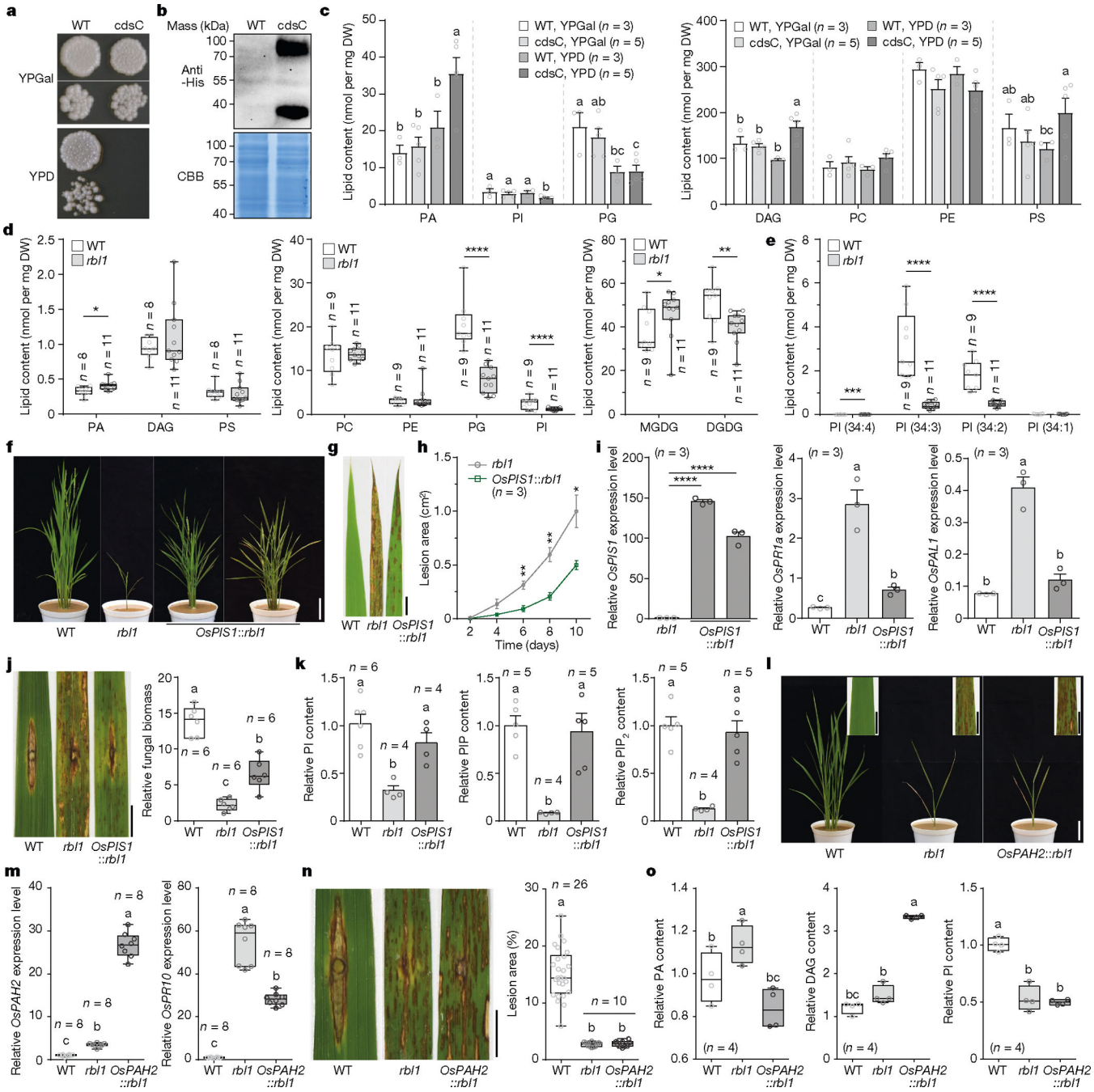

Fig. 2 |. RBL1 functions as a CDP-DAG synthase.

a, *RBL1* rescues the growth defect of the yeast *cds1* mutant (images show growth on YPGal and YPD medium). WT, yeast strain BY4741; cdsC, yeast mutant *cds1* expressing *RBL1*. **b**, Immunoblotting analysis of the RBL1–6×His fusion protein (monomeric and dimeric states). CBB, Coomassie brilliant blue. Similar results were obtained from three independent experiments. **c**, Lipidomics assays of yeast strains cultured in YPGal or YPD. DW, dry weight; DAG, diacylglycerol; PA, phosphatidic acid; PC, phosphatidylcholine; PE, phosphatidylethanolamine; PG, phosphatidylglycerol; PI, phosphatidylinositol; PS,

phosphatidylserine. **d**, Lipidomic analysis of the 4-week-old wild-type (WT, Kitaake) and *rbl1* lines. MGDG, monogalactosyldiacylglycerol; DGDG, digalactosyldiacylglycerol. **e**, Fatty-acid species of PI. No alterations were detected between WT and *rbl1* for fatty-acid species 36:1 to 36:6. **f**, Eight-week-old T_1 plants of the *OsPIS1* overexpression *OsPIS1*::*rbl1* lines. Scale bar, 10 cm. **g**, Lesions on new rice leaves. Scale bar, 1 cm. **h**, Lesion area of the lines shown in **g**. **i**, RT–qPCR assays of genes in the *OsPIS1*::*rbl1* line. **j**, Punch inoculation with *M. oryzae* and relative fungal biomass at 14 dpi. Scale bar, 1 cm. **k**, Lipid content for PI, phosphatidylinositolphosphates (PIPs) and PtdInsP_2 (PIP_2). **l**, Eight-week-old plants. *OsPAH2*::*rbl1*, the *rbl1* line overexpressing *OsPAH2*. Black scale bar, 1 cm; white scale bar, 10 cm. **m**, RT–qPCR assays. **n**, Punch inoculation with *M. oryzae* and the lesion area at 14 dpi. Scale bar, 1 cm. **o**, Lipidomics assays of different rice lines. Data are mean ± s.e.m.; *n* is the number of biologically independent samples in the graphs. Asterisks in **d**,**e**,**h** and **i** indicate significant differences using the two-tailed Student's *t*-test (*$P < 0.05$, **$P < 0.01$, ***$P < 0.001$, ****$P < 0.0001$). For exact *P* values, see Source Data. The box plot elements are: centre line, median; box limits, 25th and 75th percentiles. Significant differences indicated by letters in **c**, **i**–**k** and **m**–**o** were calculated using the Duncan's new multiple range test.

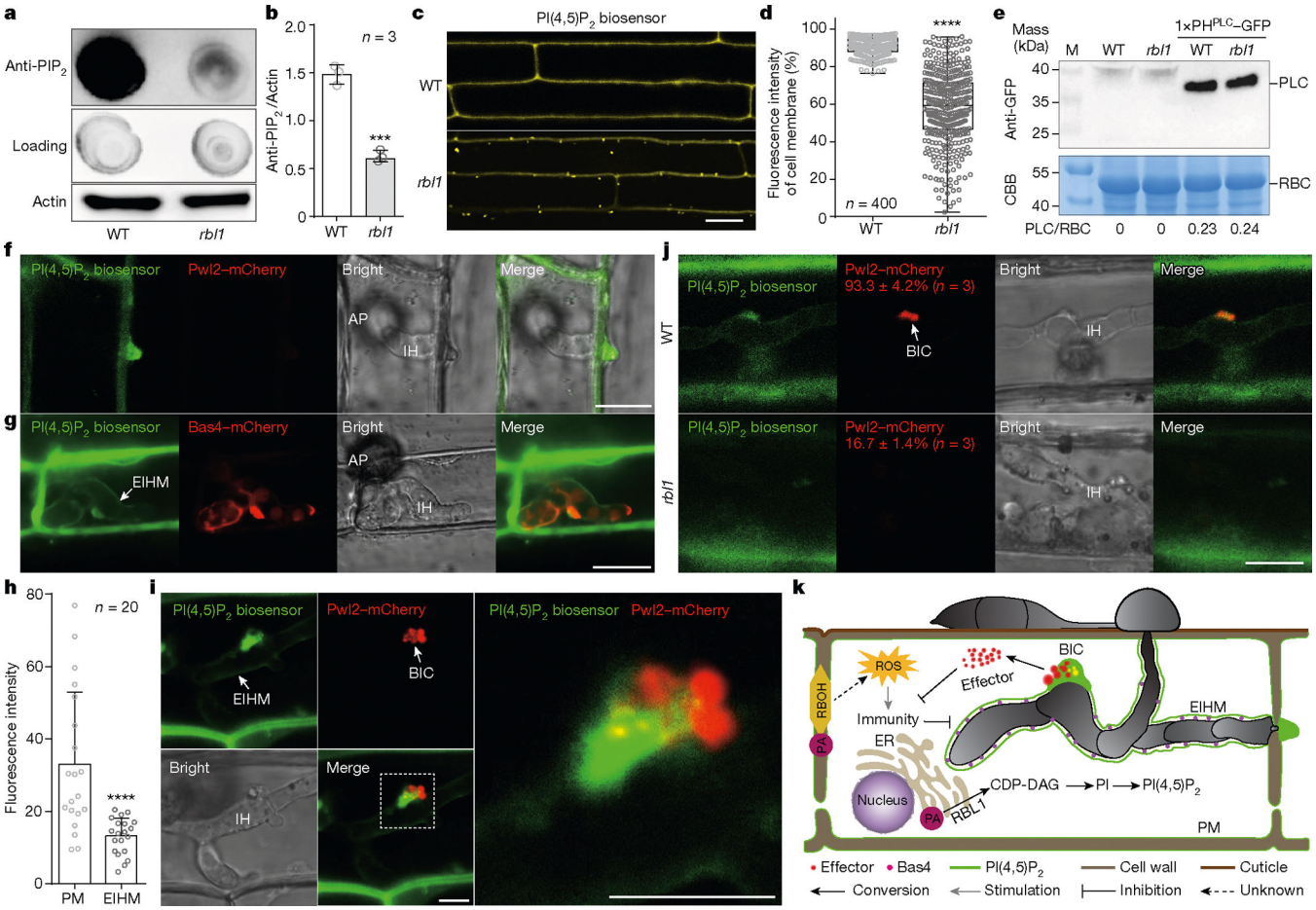

Fig. 3 |. PtdIns(4,5)P_2, enriched in infection-specific structures, is reduced in *rbl1* plants.

a, Dot blots of membrane PIP_2 in the WT (Kitaake) and *rbl1* lines. **b**, Relative levels of membrane PIP_2. Actin was used as the sample control. **c**, Epidermal cells of rice lines expressing the PtdIns(4,5)P_2 (PI(4,5)P_2) biosensor. Scale bar, 25 μm. **d**, Relative fluorescence intensity of the PI(4,5)P_2 biosensor in **c**. The box plot elements are: centre line, median; box limits, 25th and 75th percentiles. **e**, Immunoblots of the PtdIns(4,5)P_2 biosensor in **c**. M, molecular-weight marker; PH^{PLC}, the pleckstrin homology domain of PLCδ1; PLC, the biosensor phospholipase C; RBC, ribulose-1,5-bis-phosphate carboxylase/oxygenase. **f**, PI(4,5)P_2 aggregates around the infectious hyphal tip of *M. oryzae* at 22 hpi. AP, appressorium; IH, invasive hyphae. Pwl2 is a cytoplasmic effector, a biomarker for the BIC. Scale bar, 10 μm. **g**, Rice cells of the WT expressing the PI(4,5)P_2 biosensor infected by the *M. oryzae* strain expressing the fluorescent apoplastic effector Bas4–mCherry at 27 hpi. Scale bar, 10 μm. **h**, Fluorescence intensity of the plasma membrane and EIHM shown in **g**. **i**, PI(4,5)P_2 and Pwl2 at the BIC at 32 hpi. The inset shows the enlarged BIC. Scale bars, 5 μm. **j**, BIC formation rates from 150 infected cells. Scale bar, 10 μm. Experiments were repeated three (**e**) or more (**f**,**g**,**i** and **j**) times with similar results. **k**, Working model of how RBL1 confers rice resistance to *M. oryzae*. RBL1 is important for the biosynthesis of phosphatidylinositol and phosphatidylinositolphosphates including PI(4,5)P_2. As *M. oryzae* invades, PI(4,5)P_2 is recruited to the EIHM and enriched in the

BIC. The accumulation of phosphatidic acid, a minor factor, and other unknown factors contribute to the enhanced immunity of *rbl1*. ER, endoplasmic reticulum; PM, plasma membrane. Data are mean ± s.d. (**j**) or mean ± s.e.m.; *n* is the number of independent replicates (**b**) or biologically independent samples (**d** and **h**). Asterisks indicate significant differences using the two-tailed Student's *t*-test (***$P < 0.001$, ****$P < 0.0001$). For exact *P* values, see Source Data.

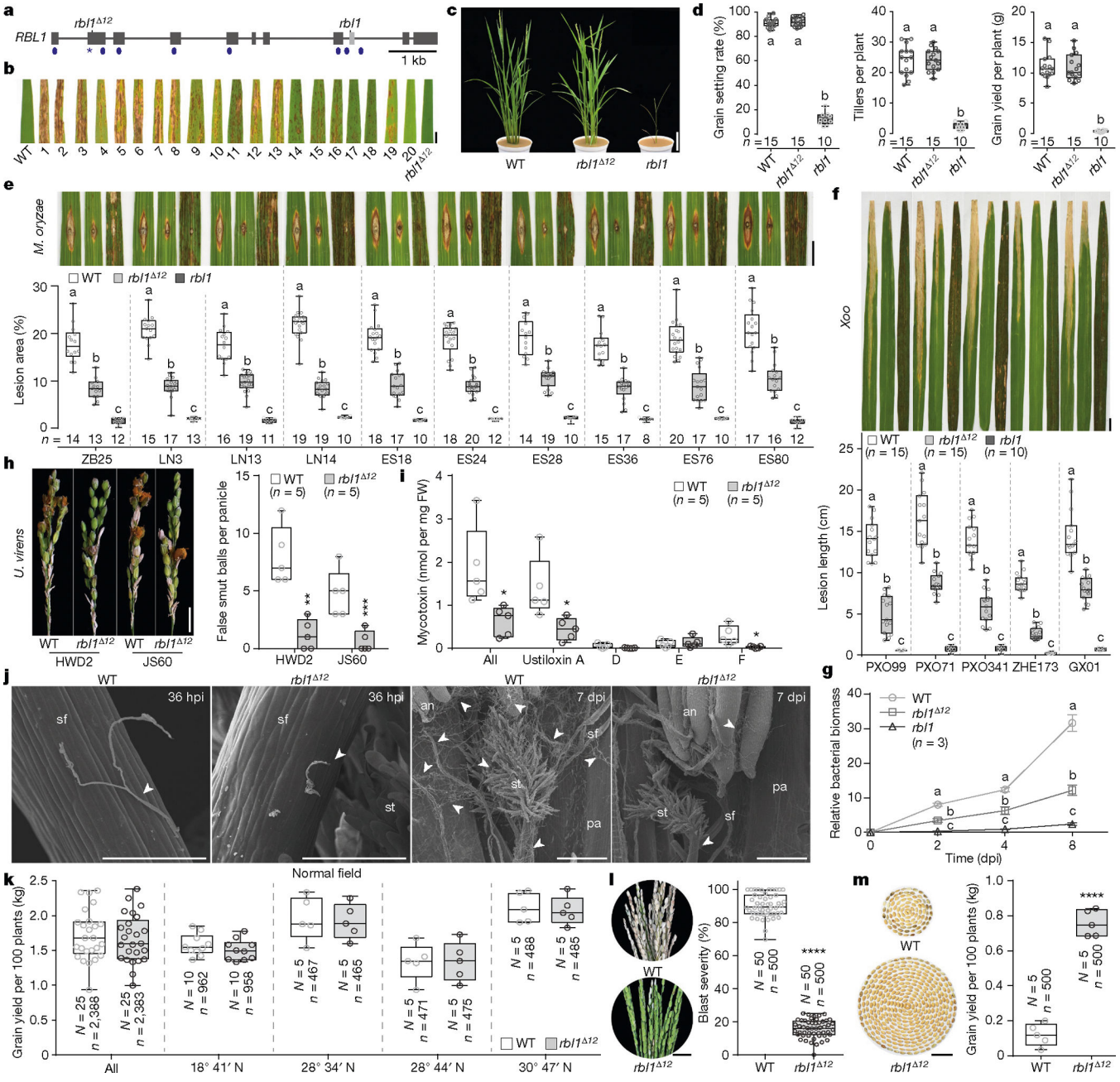

Fig. 4 |. *RBL1*$^{\Delta 12}$ confers broad-spectrum disease resistance with no observed yield penalty in field trials.

a, Guide RNA sites, indicated by dots, for genome editing of *RBL1*. The asterisk indicates the edited site in *rbl1*$^{\Delta 12}$. **b,** Edited *RBL1* lines. Scale bar, 1 cm. **c**, Eight-week-old plants in the greenhouse. Scale bar, 10 cm. **d**, Agronomic traits: grain setting rate, number of tillers and grain yield. **e**, Lesions from different *M. oryzae* strains at 14 dpi. Scale bar, 1 cm. **f**, Lesions from various *Xoo* strains at 14 dpi. Scale bar, 1 cm. **g**, In planta bacterial growth of *Xoo* strain PXO99. **h**, Panicles infected with strains of *U. virens*. Rice false smut balls were counted at 17 dpi. **i**, Quantitative assays of ustiloxins from *U. virens* in infected panicles. FW, fresh weight. **j**, Spikelets infected with strains of *U. virens*. Arrows indicate

invasive hyphae. an, anther; pa, palea; sf, stamen filament; st, stigma. Scale bars, 100 μm. Experiments were repeated twice with similar results. **k**, Rice grain yield in the 'normal' field trials with a low incidence of rice blast. **l**, Field assessment of blast resistance in the blast nursery. Representative panicles are shown on the left. Disease severity is indicated by the percentage of necrotic panicles for each plant caused by *M. oryzae* infection. Scale bar, 1 cm. **m**, Grain yield of plants grown in the blast nursery. Seeds per plant are shown on the left. Scale bar, 1 cm. The box plot elements are: centre line, median; box limits, 25th and 75th percentiles. Data are mean ± s.e.m.; *n* is the number of biologically independent samples in the graphs. Asterisks indicate significant differences using the two-tailed Student's *t*-test (*$P < 0.05$, **$P < 0.001$, ***$P < 0.001$, ****$P < 0.0001$). For exact *P* values, see Source Data. Significant differences indicated by different letters in **d**–**g** were calculated using the Duncan's new multiple range test.